SEAFLOOR PROCESSES AT KICK ‘EM JENNY VOLCANO, PRE- JULY 2015 VOLCANIC EVENT, USING HIGH-RESOLUTION SHIPBOARD AND REMOTELY OPERATED VEHICLE NEAR-SOURCE DATA

A Thesis

by

TYLER LOUIS RUCHALA

Submitted to the Office of Graduate and Professional Studies of
Texas A&M University
in partial fulfillment of the requirements for the degree of

MASTER OF SCIENCE

Chair of Committee,	Masako Tominaga
Committee Members,	Brent Miller
	Jason Sylvan
Head of Department,	Michael Pope

May 2017

Major Subject: Geophysics

ABSTRACT

To understand the physical and geological processes that drive the volcanism and control the morphology of KEJ volcano, the only active submarine volcano in the Lesser Antilles volcanic arc, I conducted near-source, high-resolution bathymetry and magnetic mapping of KEJ volcano and its subsurface using the ROV *Hercules* during cruise NA054 of the E/V *Nautilus* (Sept.-Oct. 2014). In our results, multiple generations of submarine landslides and well-developed canyons are observed, suggesting that the area has been hosting dynamic sediment transport systems from the flank of the volcano to the seafloor at multiple scales over time, with some of them being attributed to past eruptions. The canyons likely formed from in situ gravity flows due to the lack of evidence for subsidence in the area of KEJ. Columnar basalts located in the middle of the landslide deposit are similar in appearance to those observed in the KEJ crater during previous ROV dives, indicating a possible extent of a landslide event, i.e. a travel distance of volcanic materials from the crater region along landslide path. Landslide triggers at KEJ are still debated, but sector collapse of the edifice has been numerically predicted to be the failure style. High-resolution near-bottom magnetic anomaly data is used to investigate ongoing volcanism at KEJ, and revealed a magnetic anomaly high within the inner crater of KEJ. The source of the dichotomy in magnetization is both a dike complex at the inner crater and a fault trending NNE-SSW. I propose the following cyclic evolution scenario of KEJ from eruption events to inter-eruption periods, by

combining seafloor morphology observations, integrating high-resolution bathymetry maps, ROV visuals and rock samples from the wholesale KEJ, and subsurface characterization with high-resolution near-bottom magnetic survey of KEJ crater and inner crater. KEJ formed from arc volcanism; the magma rises quickly though the magma conduits to the shallow subsurface with a series of dikes; it erupted in shallow water depth; it erupted in an explosive style; these volcanic eruptions trigger a landslide and deposit material downslope; submarine canyons form from in situ submarine gravity flows until next the eruption.

DEDICATION

Thank you to all those that supported me though my geology journey. Beginning with my dad who took me camping and allowed me to discover my passion for rocks. Finishing with the most recent supporter, at the time of writing, Dr. Masako Tominaga who helped me focus in on geophysics and appreciate rocks for more than just their aesthetic appeal.

"Comfy in Nautica."

-- Panda Bear

ACKNOWLEDGEMENTS

I thank the fellow participants in TREET that made this possible. I acknowledge support from the Ocean Exploration Trust (Cruise NA054 of the E/V Nautilus). Data relating to this work are available from the following source: ROV data from NA054 by request through the Inner Space Center at the Graduate School of Oceanography, University of Rhode Island, USA (Dwight Coleman: dcoleman@gso.uri.edu).

CONTRIBUTORS AND FUNDING SOURCES

This work was supervised by a thesis committee consisting of Professor Dr. Masako Tominaga and Dr. Brent Miller of the Department of Geology and Geophysics and Professor Dr. Jason Sylvan of the Department of Oceanography.

All work for the thesis was completed by the student, in collaboration with Dr. Steve Carey of the Graduate School of Oceanography at The University of Rhode Island, and Dr. Frédéric Dondin of the Seismic Research Centre at The University of the West Indies.

This work was made possible in part by National Science Foundation under Grant Number OCE-1258771.

Its contents are solely the responsibility of the authors and do not necessarily represent the official views of the National Science Foundation.

NOMENCLATURE

A/m	ampere/meter
BP	before present
C	Celsius
cm	centimeter
D	headscarp height
E	east
H	height of fall
HD	high-definition
Hz	hertz
IGRF	International Geomagnetic Reference Field
KEJ	Kick ‘em Jenny
km	kilometers
kyr	thousand years
L	runout
m	meters
N	north
mbsl	meter below sea level
NNE	north-northeast
nT	nanotesla
RMSE	root mean square error

ROV	remotely operated vehicle
S	south
SSW	south-southwest
TMI	total magnetic intensity
μm	micrometer
USBL	ultra short baseline
W	west
°	degree

TABLE OF CONTENTS

LIST OF FIGURES

LIST OF TABLES

1. INTRODUCTION

Submarine volcanism provides evidence for understanding Earth's planetary evolution. About 90% of the annual output of the magma budget on Earth is produced at the seafloor (White et al. 2006), rendering submarine volcanism an important component of the planetary-scale energy budget and thermal evolution of Earth (Crisp, 1984; White et al. 2006). Volumetrically, the most pronounced submarine volcanism is globally observed in the form of seafloor spreading at mid ocean ridges (Crisp, 1984; Haymon et al. 1993; Sinton and Detrick, 1992; Speight and Henderson, 2010; White et al. 2006) and of numerous seamounts and igneous provinces within intra plate settings (Clouard and Bonneville, 2001; Wessel, 1997; Wilson 1963), convergent plate boundaries (Speight and Henderson, 2010) and rifting margins (Larsen and Saunders, 1998). Submarine volcanism is often associated with landslides when the sediment blanket has thickened over time (Bell et al. 2013; Boudon et al. 2007; Dondin et al. 2012; Siebert et al. 1987; Silver et al. 2009; Watt et al. 2012; White et al. 2006). Understanding the nature and behavior of submarine volcanoes allows us to assess Earth's magmatic events in time and place (Bleeker and Ernst, 2006; Kay and Kay, 1993), their environmental impacts (Eldholm and Thomas, 1993; Jones and Jenkyns, 2001; Stothers, 1993), as well as the tsunamigenic potential of underwater landslides (Dondin et al 2017, 2012; Watt et al. 2015), which becomes a significant geohazard, especially areas near large human populations (Cummins, 2007; McAdoo et al. 2009; Polet and Kanamori, 2000).

Devastating natural disasters can be caused by submarine landslides (Locat and Lee, 2002; Masson, 2006; Smolka, 2006), with different inherent risks based on the landslide's location relative to human activity (Randolph and White, 2012). Submarine landslides are commonly observed in the continental shelves (Bryn et al. 2005; Masson et al. 2006; Twichell et al. 2009), the flank of oceanic islands (Heinrich et al. 1998), and submarine volcanoes (Carey et al. 2016; Dondin et al. 2012; Watt et al. 2015; Watt et al. 2012) (Table 1). Submarine landslides on the continental slope pose a direct hazard to the deepwater pipelines that transport hydrocarbon (Kvalstad et al. 2001; Randolph and White, 2012). Large-scale landslides are a key process in the evolution of oceanic islands (Masson et al. 2002), such as Hawaii (Moore et al. 1994), La Reunion (Masson, 1996; Lenat and Aubert, 1982), and the Canary Islands (Masson, 2002; Masson, 1996) where material from the islands can be transported hundreds of km and cover hundreds of km^2 of the seafloor (Masson et al. 2006; Masson et al. 2002). Although possible impacts by such submarine geological process can make a significant impact on human society, characterizing the submarine landslide occurrence in space and time has been merely discussed. Investigating characteristics of the landslide activities from topographic observations and rock samples that were involved in the landslide can provide insight into the emplacement processes of a landslide (Horbitz et al. 2006; Watt et al. 2012) and, in turn, geological processes that induced the landslides (Watt et al. 2015; Watt et al. 2012).

In determining the source of the material, lithology and structure of the landslide material from high-resolution and systematic observations, particularly in the case of

Location	Failure type	Volume (km^3)	Velocity (m/s)	Environmental Impact	Tectonic Setting	Reference
Storegga Slide (Norway, ca. 8200 years ago)	Earthquake, sediment loading, and Gas hydrate melting	2500-3500	10-20	Catastrophic impact on the Mesolithic population in the area	Continental shelf	Bryn et al. 2005
Nuuanu (Hawaii, 1888)	-	5000	-	-	Hot Spot	Masson et al. 2006
Great Banks (Canada, 1927)	Slope Failure and Earthquake	100-150	15-30	Broke submarine cables	Stable mid continent	Fine et al. 2005
Unimak (Alaska, 1946)	Earthquake and Slope Failure	-	199	-	Aleutian Subduction Zone	Watts et al. 2005
Seward (Alaska, 1964)	Earthquake induced landslides	.211	-	Destruction to the city of Seward	Aleutian Subduction Zone	Suleimani et al. 2011
Kitimat Arm (Canada, 1975)	Failed mass	.055	17-22.5	-	-	Skvortsov et al. 2007
Nice Failure (Mediterranean Sea, 1979)	Submarine Slide	0.0087-0.07	-	-	-	Assier-Rzadkiewicz et al. 2000
Skagway (Alaska, 1994)	Various Landslides	0.003-0.01	31-35	Destroyed railway dock	Aleutian Subduction Zone	Watts et al. 2005
Montserrat (Lesser Antilles, 1997)	Debris Avalanche	0.04	30-40	-	Volcanic Island Arc	Heinrich et al. 1998
Papuaa New Guinea (1998)	Underwater Slump and Earthquake	6	11.4	20 km of coast affected	Subduction zone	Watts et al. 2005
Izmit Bay (Turkey, 1999)	Earthquake Induced Slides	-	2.4	-	Active plate margin	Watts et al. 2005
Chehalis Lake (Canada, 2007)	Subaerial landslide	.003	-	Extensive shoreline damage	-	Roberts et al. 2013

Table 1. Historical Documented Landslides. Historical landslides catalog highlighting the key attributes of the different landslides.

submarine volcanoes, outcrop scale geophysical remote sensing are imperative to accurately characterize textures and lithologies of the deposits. These techniques can help determine the provenance of the material, and informs the transportation processes that occurred (e.g. Carey et al. 2016; Day et al. 2015; Watt et al. 2015; Watt et al. 2012). Based on the near-source characterization of the seafloor features and rocks involved in the landslide, as example, Watt et al. (2012) deciphered the relative timing between the landslides to occur offshore Montserrat, Lesser Antilles, and the triggering mechanism for the landslides. Despite the widely recognized significance of advancing our knowledge on submarine volcanism and associating material transport as a consequence of planetary magmatism however, their eruption mechanisms, let alone, their origin and environmental impacts at different timescale –whether landslides are attributed to the eruption of underwater volcano, inflation of the ground inducing instability or gravity flows induced by the fault instability and whether how material transport due to the slides have operated have merely been discussed.

In this study, I examine the nature of KEJ submarine volcano and associated landslides using shipboard multibeam data, high-definition video, and photomosaics from the crater of KEJ volcano, midslope and toe of the landslide. Our findings provide new evidence and implications for the provenance and processes of the landslide and volcanic activity at KEJ, in time and space, and will suggest in situ geological processes only a year prior to its most recent eruption event.

2. BACKGROUND

2.1 Submarine Volcanoes

Numerous submarine volcanoes have been identified based on satellite altimetry and gravimetry data (Hillier and Watts, 2007; Speight and Henderson, 2010; Wessel, 2001). The number of estimated submarine volcanoes, which is based on minimum size (e.g at least 1 km above seafloor), on the ocean floor range from 100,000 (Wessel, 2001) to 1 million (Speight and Henderson, 2010) to 3 million (Hillier and Watts, 2007). Some of the submarine volcanoes are in shallow water. Submarine volcanoes located in shallow waters have the potential for explosive and hazardous eruptions as a result of the lower pressure exerted on the crater from the above water column (Fagents et al. 2013).

Magma composition at submarine volcanoes varies, and different hazards are associated with different magma composition, depending on tectonic setting the volcano forms on. Submarine volcanoes are typically found at plate boundaries, and hot spots (Hillier and Watts, 2007; Speight and Henderson, 2010). The largest concentrations of active submarine volcanoes are found on arcs in subduction zone settings (Watts et al. 2012). At all three of these areas basaltic magma can be produced, but if a convergent boundary or hot spot erupt on continental crust, andesitic magmas predominate (Tatsumi, 2005). There is an additional hazard associated with that due to the higher volatile percentage (Sigurdsson et al. 2006), making these volcanic eruptions more explosive. Identifying what tectonic setting the submarine volcanism is occurring on

provides insight into the magma composition and the different hazards with the different magma types.

Hazards associated with shallow water submarine volcanoes include tsunamis, lowered water density above the crater, and ballistic projectiles (Lindsay et al. 2005). Tsunamis can occur by the displacement of a large amount of mass downslope during a submarine landslide, inducing tsunami waves (Dondin et al 2012). Lowered water density is caused when there is a large release of gas into the water during magma degassing (Lindsay et al. 2005). Ballistic projectiles can emerge from the sea and be propelled up to 5 km from the volcano, posing danger to nearby ships (Lindsay et al. 2005). The damages caused by submarine landslides have been well documented to have devastating impacts on people and infrastructure (Locat and Lee, 2002; Masson, 2006; Smolka, 2006).

Once a submarine volcano or seamount is identified, different techniques are used to visualize the morphology and architecture of the submarine volcano. Shipboard multibeam has been the preferred data source for mapping, identifying and sampling submarine volcanoes and their associated features (Horbitz et al. 2006; Machida and Ishii, 2003; Watt et al. 2012). Shared features of a submarine volcano and landslide are: a caldera, levees, scarp, and toe (Carey et al. 2016; Dondin et al. 2012; Watt et al. 2015; Watt et al. 2012). Dredges have historically been used to collect samples from submarine volcanoes (Machida and Ishii, 2003). Recent development of integrated surveying techniques utilize ROVs and Autonomous Underwater Vehicles to record videos of key geologic features, collect rock samples, and measure high-resolution geophysical data of

the underwater landslide (Carey et al. 2016; Day et al. 2015; Watt et al. 2015). Identifying key features associated with submarine landslides, using bathymetric and ROV-based data, is the first step in characterizing a submarine landslide and the failure that caused the landslide.

TMI data provides insight into present day volcanic and geologic processes occurring at the volcano's caldera. Aeromagnetic data has been used to characterize the magmatic source of submarine volcanoes (Lenat and Aubert, 1982; Malahoff and Wollard, 1968). While in recent years, magnetometers have been attached to submersibles to obtain high-resolution magnetic anomaly data, which are used to provide constraints to detect hydrothermal activity, study the hydrothermal activity's affect on the magnetization value of the basalt and andesite hosted rocks and to investigate study the magnetic structure of a slow spreading ridge (Fujii et al. 2015; Honsho et al. 2009; Szitkar et al. 2015a; Szitkar et al. 2015b). Due to the active geologic processes occurring at the volcano's caldera, the passive nature of the magnetic dataset allows us to capture the geological processes and quantify the geological processes (Tivey and Johnson, 1989).

2.2 Geologic Background of Kick 'em Jenny

KEJ volcano (Fig. 1), is the only active submarine volcano in the Lesser Antilles, and has been investigated previously by (Carey et al. 2016; Carey et al. 2014; Devine and Sigurdsson, 1995; Dondin et al. 2012; Lindsay et al. 2005; Sigurdsson and Shepherd, 1974). It is located approximately 8 km northwest of the island of Grenada

(Fig. 1). KEJ volcano formed from arc volcanism and primarily consists of amphibole bearing andesitic basalt (Devine and Sigurdsson, 1995; Sigurdsson and Shepherd, 1974). Amphibole is an important mineral because breakdown rims will form on the outside of the amphibole grains as the magma ascends to the surface due to decrease in melt water percentage (Devine et al. 1998; Devine and Sigurdsson, 1995). This decease in water percentage tends to cause reactions between the amphibole phenocryst and melt, and the extent of the reaction is a function of decompression rate, which is proportional to the ascension rate of the magma (Geschwind and Rutherford, 1995; Rutherford and Hill, 1993). The thicker (200-400 μm) the breakdown rim, the longer it took the magma to ascend to the surface (Devine et al. 1998; Devine and Sigurdsson, 1995).

Based on 2014 shipboard bathymetry data, KEJ volcano has the following dimensions: 1300 m thick from toe to the cone, a 320 m radius crater, a 100 m radius inner crater, located in the north central portion of the crater, and the summit is 185 m below the sea level. From the top of the Kick ‘em Jenny crater (ca. 185 m) to the toe of associated landslide (ca. 2500 m) is 14 km (Fig. 2). The scarp of KEJ opens to the west-northwest towards the Grenada Basin.

2.2.1 Volcanic Activity at Kick ‘em Jenny Pre- 2014

KEJ is a premier location to study the interaction between submarine volcanism and associated landslides because of the known and frequent eruption history. When seismic activity began recording in 1939, there has been a documented seismic swarm every 6 years near KEJ location (Devine and Sigurdsson, 1995; Lindsay et al. 2005) with

the most recent volcanic activity occurring June 2015 (Robertson et al. 2015). The ancestral KEJ volcano is modeled to appear ca. 230 meters above sea level and have gone through at least one major landslide event (Dondin et al. 2012), with a possibility of two additional landslide events. In August 1944, the Island Queen, a wooden schooner, was sunk due to lowered water density over KEJ crater, highlighting the hazards and need to monitor KEJ.

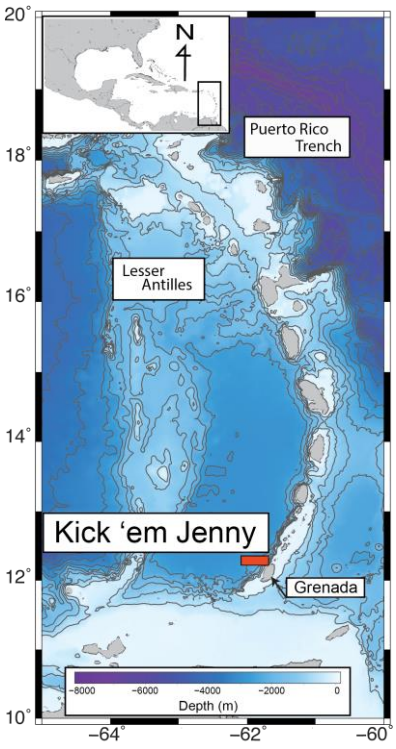

Figure 1. Map of Study Area. A map showing Kick 'em Jenny location (red rectangle) within the Lesser Antilles island arc chain. Underlying seafloor topography is based on satellite altimetry (Smith and Sandwell 1997).

2.2.2 Onshore Record of Tsunamis in Grenada and St. Lucia

There are two locations on the island of Grenada where there are paleo-tsunami relics (Scheffers et al. 2005), that provides additional support that a tsunami has occurred in the area. In the northwest area of the island, there is bimodal stratum of sandy matrix with well-rounded cobbles and boulders within a pyroclastic strata (Scheffers et al. 2005). On the west coast, there is a 200 m long boulder ridge with steep flanks (Scheffers et al. 2005). It is likely this is not a man made feature according to specialists in the field Antillean prehistory (Bullen, 1964). Rendering the placement of these boulders as another paleo-tsunami relic.

There is also evidence for tsunamis on the islands of St. Lucia, 200 km north of Grenada, (Scheffers et al. 2005). On the west coast of St. Lucia, there is thick stratum of chaotic mixture of very fine particles with gravel and boulders, with weights up to 10 tons, which represents paleo-tsunami relic in the pyroclastic stratigraphy (Scheffers et al. 2005). Based on weather son the boulders, they could surmise that these were deposited during the Middle Pleistocene. Although it could not be determined where exactly the tsunami that caused these relics originated from, it is interested to note that they are all deposited on the west coast of the islands, indicating that the tsunami did not originate from the Atlantic Ocean and move westward the Antilles Island arc (Scheffers et al. 2005).

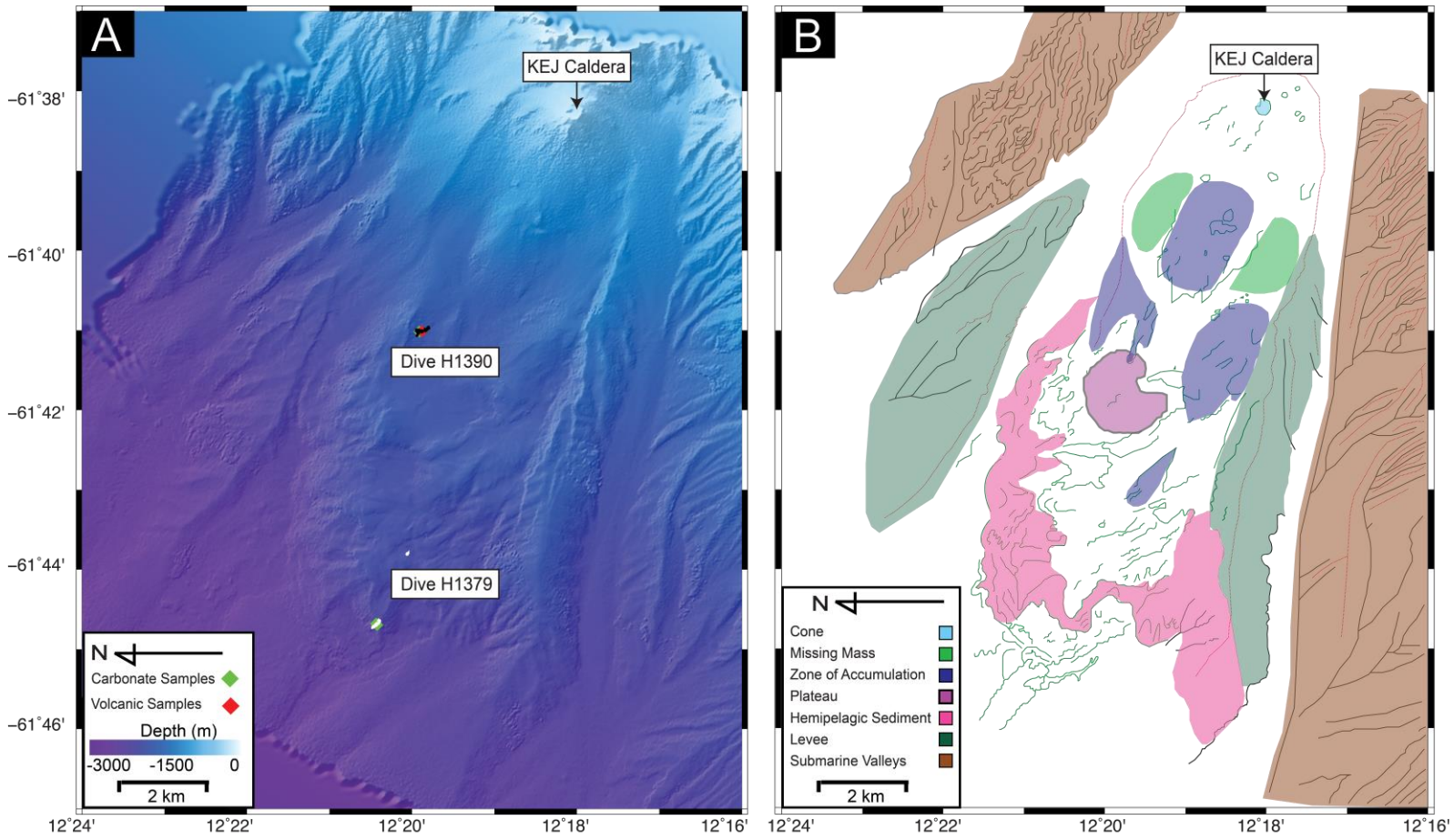

Figure 2. Bathymetry and Interpretation Map. (A) Shipboard bathymetry map displaying the distribution of the different rock samples and the track of the ROV during the two different dives. (B) Different geologic and morphological interpretations of the landslide. Green lines represent steep subtle changes in the slope, red represents ridge apexes, and black represents submarine valleys.

3. METHODS

3.1 Multibeam Bathymetry Acquisition and Data Analyses

High-resolution shipboard swath bathymetry data was collected with a Kongsberg EM302 system during NA054 cruise on the Ocean Exploration Trust's *E/V* Nautilus (Sept. – Oct. 2014). The data covers the entire landslide ca. 4.4 km^2 (Dondin et al. 2012). I used the multibeam data to create a bathymetry map (Fig. 2A), and to create the slope direction and angle maps, which is extracted from the bathymetry map (Fig. 3A and 3B). These data provided a new perspective on the morphology of the landslide; which is not seen strictly looking at the bathymetry map. These three maps provide details about the morphology of the landslide, which are shown in detail (Fig. 2B). Bathymetric data highlights the seafloor expression of these landslides, but distances can be measured from these maps, which can be used to predict how the imaged landslide behaved.

Landslides have quantitative ratios that can allow us to predict how the landslide behaved during failure. The mobility of the second-generation landslide can be predicted by the ratio between the height of the fall and the runout (Hayashi and Self, 1992). Additionally, the rheology of the material can be highlighted by the ratio between headscarp height to runout (Crozier, 1973). Mobility and rheology are two factors that go into assessing how a submarine landslide behaved. Another important factor is the volume of material moved during the failure.

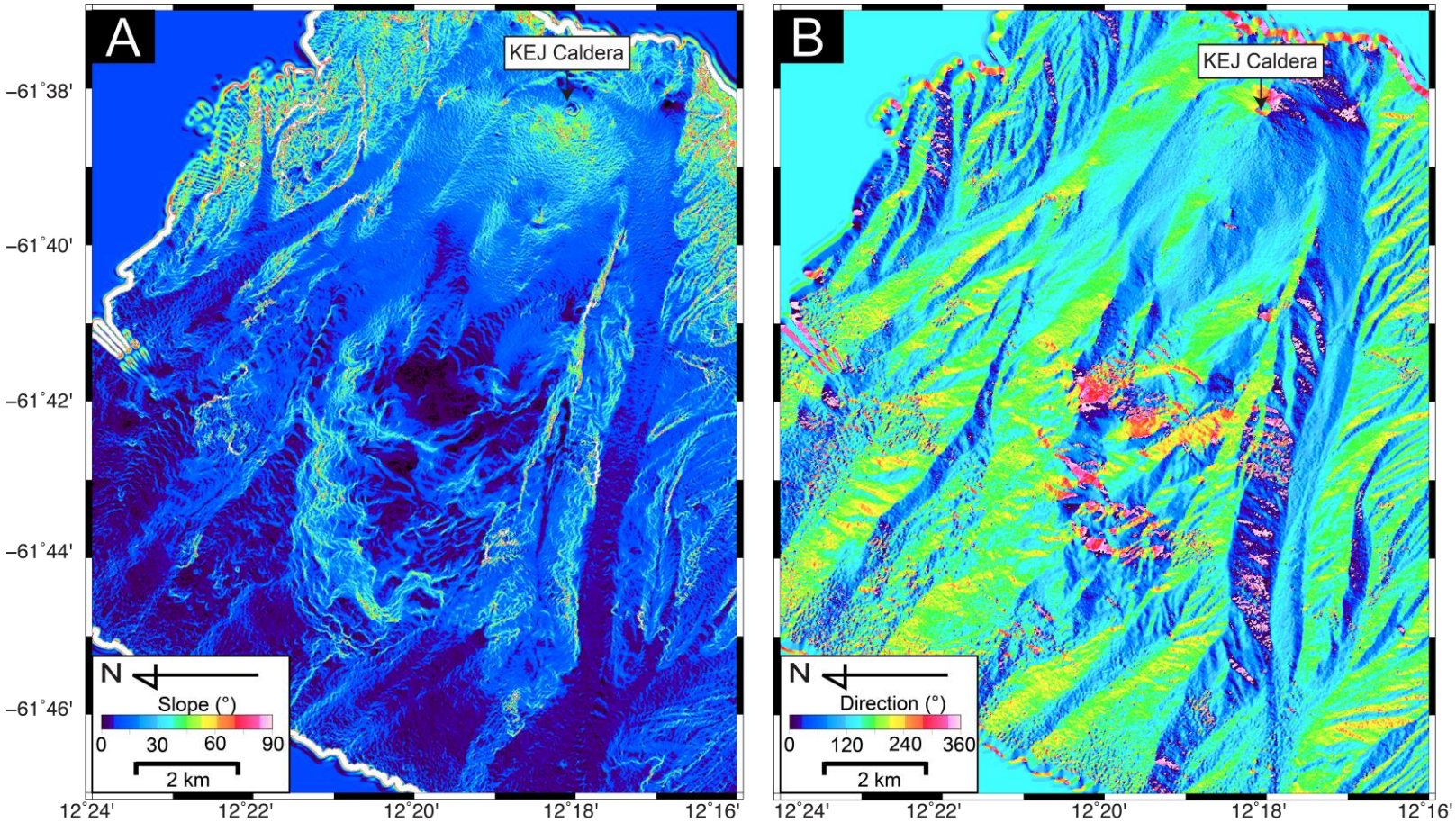

Figure 3. Slope and Directions Maps. Maps derived from the bathymetric data: (A) Slope angle map of the landslide that is displaying the steepness of the slopes at each location. (B) Upslope direction map that displays the direction of the landslide slopes.

The area of a landslide can has been used to determine the volume of material involved in the same landslide. The volume and the area of the second-generation landslide is known, which allowed us to determine which empirical relationship between the landslide area and volume best fit at KEJ. This empirical relationship is applied to the area covered by the third generation landslide to determine the volume. The equation used:

$$\text{Volume} = (0.769)(\text{Area})^{1.250} \text{ ------- (1)}$$

is determined from 45 different landslides to develop this relationship (Whitehouse, 1983).

3.2 Near-Bottom High-Resolution Videos and Geological Mapping

ROV Hercules collected high-definition videos and rocks samples, which are used to support our overarching goals. Dives H1379m H1380, and H1390, lasted eight hours each. I used digital still images, high-definition videos, and rock samples to examine the crater of the volcano, toe, and midslope of the landslide. Dive H1390 was designed to investigate a contact between volcanic rocks from the edifice of the volcano and newly lithified carbonate rock at the midslope. The ROV collected carbonate samples that are in contact with the volcanic rock to perform Accelerator Mass Spectrometry on the foraminifera in the carbonate rock, to determine a potential age constraint on a landslide deposit. In order to utilize in situ observations efficiently, knowing exactly where the samples and observations are located on the landslide is

paramount. I located all the visual data because it was merged with USBL navigation data between ship and ROV Hercules based on time stamps.

Still images from the ROV were merged to create 47 photomosaics using the photomerge tool in Adobe Photoshop. Notable shared features in consecutive still images were used to determine alignment to create a coherent, continuous mosaic. Gathering visual aids on how the landslide is deposited provides insight into the processes that occurred, which leads to how the material in the landslide is transported. Additionally, geologic mapping of bacterial mats, hydrothermal vents, and geologic material in the crater is done to allow us to interpret fluid flow in the system, and to create a baseline to correlate changes in volcanic activity.

3.3 Near-Bottom Magnetic Mapping

High-resolution TMI data from the inner crater of the Kick ‘em Jenny Volcano has been collected during two ROV dives which added up to be 144-hours of data and a total of 18 profiles. The magnetometer that is attached to the ROV is the Honeywell HMR 2300, and it measures the X, Y, and Z vector components of the magnetic field.

The raw magnetic data is corrected for vehicle induced magnetic noise, and then merged with ship navigation data at 1 Hz. The magnetic data is also corrected for the IGRF (Thébault et al. 2015) and diurnal variations, using data from the San Juan Magnetic Observatory (http://geomag.usgs.gov/monitoring/observatories/sanjuan/) and adjusted to survey local time. These additional corrections are made in order to better understand the crustal magnetic signatures; thus creating a true magnetic anomaly

related to the subsurface. Next, the corrected 18 2-D profile lines are linearly interpolated onto a straight line with a15-cm spacing. The remanent magnetic source has an effective inclination and declination of +33° and -14° respectively. After corrections, the magnetic data is inverted in order to obtain magnetic and geometric properties of the subsurface rocks.

The magnetic anomaly data is inverted using the Parker and Huestis, (1974) method to better understand the magnetic source distribution, and gain insight on the volcanic processes occurring within the crater. To provide information on the subsurface volcanic processes of the KEJ crater and check if the inversion returned a reasonable output, a prism forward model based on (Talwani and Heirtzler, 1964) method is implemented. This forward code enabled us to represent the magnetic architecture of the subsurface using varying magnetic distribution and prism thicknesses.

3.4 Geological Samples

I used rock samples that spanned the landslide, (cone, midslope, and toe) to obtain a complete representation of rocks involved in the landslide, ground-truth our HD video, and provide additional evidence for the formation of shallow water material (Table 2). Specifically, it is important for us to collect rock samples that were located in the cone in order to compare those cone rocks with the volcanic material that is seen downslope.

Table 2. Sample Depth and Local. Sample ID, depth and location on Dive H1379, H1380, and H139 samples.

Sample	Dive	Depth (m)	Latitude (N)	Longitude (W)
NA054-004*	H1379	2204.0	12.3420	-061.7441
NA054-007*	H1379	2203.4	12.3422	-061.7438
NA054-008*	H1379	2188.6	12.3418	-061.7438
NA054-010*	H1380	260.5	12.3013	-061.6376
NA054-011*	H1380	264.1	12.3012	-061.6376
NA054-050*	H1390	1652.0	12.3332	-061.6832
NA054-051*	H1390	1653.0	12.3332	-061.6815
NA054-053*	H1390	1651.7	12.3333	-061.6814
NA054-054*	H1390	1673.0	12.3329	-061.6815

*Rock Sample and thin sections

4. RESULTS

4.1 Seafloor Morphology

From the shipboard bathymetry data, I observed the following: a head scarp cone, toe of a landslide (with some hemiplegic sediment extending further), levee (from a previous landslide), channels on bounding the landslide deposit, eroding the northern and southern escarpment, and thin submarine canyons that deposit into the channels (Fig. 2B).

The first generation landslide of KEJ (Fig. 4B) is the largest landslide and formed a levee observed in the north. This landslide has a horseshoe-shaped collapse structure and deposits 17 km downslope, terminating in the Grenada basin. I also identified the second-generation landslide, which is the landslide, generated by a sector collapse, which is a failure of the edifice that involves the magma conduit, which shaped the current edifice. It has deformed sediments and a plateau in the mid slope that is highlighted by the slope angle map (Fig. 2A). The second-generation landslide (Fig. 4C) deposited the prominent toe feature, where chemosynthetic cold seeps occur (Carey et al. 2014) and is capable of having generated a tsunami with 15-m waves (Dondin et al. 2012). The second-generation landslide would be characterized as a rock avalanche type of failure because the H/L ratio, indicative of limited mobility of the landslide (De Blasio et al. 2006; Hayashi and Self, 1992), was ca. 0.21. The rheology was blocky-disintegrative because the D/L ratio, indicative of a more fluid landslide, not as many

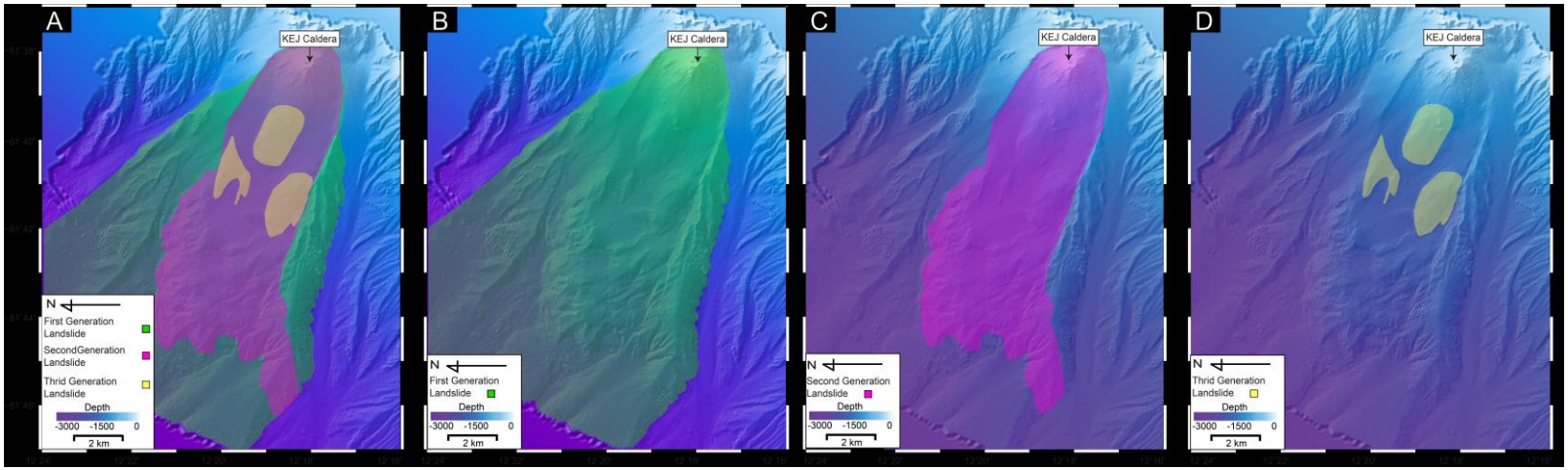

Figure 4. Distribution of Landslides Generations. (A) Shipboard bathymetry maps with interpretations showing the distribution of the three different landslides observed in the area. (B) The first generation landslide. This deposit has an additional 5 km runout that is not seen, where the landslide deposits into the Grenada Basin (Dondin et al. 2012). (C) The second-generation landslide. (D) The third generation landslide.

blocks involved in the landslide (Croizer, 1973), was ca. 0.004 (Table 3). Lastly, I identified the third generation landslide (Fig. 4D) that occurred on the top most sediments, and bounded to the midslope with a volume of 0.295 km^3. This landslide is the only deposit that has a rounded toe. Three generations of landslides are outlined on top of one another for comparison (Fig. 4A).

I observed that the bottom current of the submarine canyons and channels have significant influence on the morphology in the vicinity of Kick 'em Jenny volcano (Fig. 2A). Slope direction highlights where the possible source for these bottom currents originate from (Fig. 3B). Along the eastern edge of the southern escarpment, I see a bottom current channel and another bottom current near the mid slope of the southern escarpment. Near the north escarpment, I see the levee from an earlier landslide, next to the toe of a different landslide.

Table 3. Second-Generation Landslide Statistics. Empirical ratios to characterize the second-generation landslide at KEJ.

	Ratio	Characterization based on ratio	Implications	References
H/L	*ca. 0.21	Rock avalanche group	**Limited mobility	*Dondin et al. 2012 **De Blasio et al. 2006
D/L	ca. 0.004	Blocky-Disintegrative rheology	More fluid landslide, not as many blocks	

4.2 ROV Near-bottom Observations

We have provided new ROV visual observations that will supplement the visuals that have already been completed (Carey et al. 2016; Carey et al. 2014). In the crater, numerous bubble streams, a shallow ephemeral hydrothermal system, and bacterial mats are identified and located for future comparison. Cold seeps are also located on the talus slope and down on the toe of the landslide.

High-definition video from the ROV allowed us to document the midslope and toe of the landslide during our two dives. Photomosaics of the seafloor on the landslide during the dive are displayed (Fig. 5A). Dive H1390, covered 120 m, ranging in depths from 1700 m to 1659 m below sea level. At the midslope, I observed the contact between carbonate material and volcanic material (Fig. 5B). Rock samples NA054-053 and NA054-054 were taken at this contact.

Large blocks of highly fractured volcanic material from the crater are seen throughout the dive (Fig. 5C). Another piece of evidence that I will present is columnar basalts, which form from the unique cooling pattern of the crater (Fig. 5E). These volcanic material have a layer of sediment a few cm thick, indicating they were recently transported a distance of 7 km (Fig. 5D); distance is known because the volcanic rocks are proto crater material.

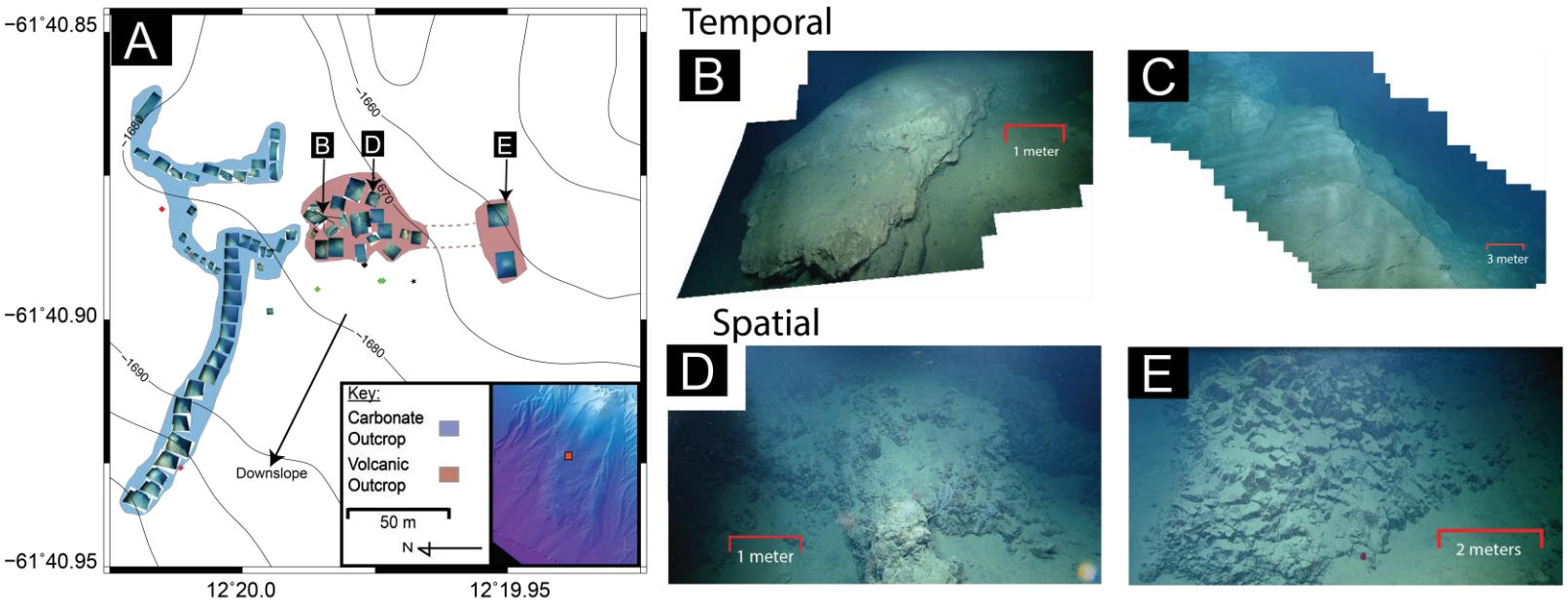

Figure 5. Focused Dive of Landslide. (A) Contour map displacing the focused dive area where I explored the nature of the volcanic and carbonate contact at ca. 1700 m. The red box in the inset map marks where this dive took place. Photomosaics from the dive were placed at their exact location with orientation based on ROV navigation and altitude data. Blue color represents seen carbonate outcrop, and red represents seen volcanic outcrop. (B) Contact between carbonate and volcanic material. (C) Thick, lithified section of carbonate outcrop. (D) Highly fractured volcanic material that that was observed at the midslope of the second-generation landslide. (E) Columnar basalt that was observed at the midslope of the second-generation landslide.

4.3 Near-Bottom Magnetic Mapping, Inversion and Forward Modeling Results

I observe a positive magnetic anomaly within the inner crater of the KEJ crater, with the magnetic intensity decreasing on the eastern half of the crater (Fig. 6D). There is a semi linear trend that runs NNE-SSW through the center of crater.

The inversion results provide the simplest solution of the 2-D magnetization distribution model for a varying thickness magnetic source layer. There is a strong correlation between the positive magnetic anomaly and positive magnetization value. At the inner crater, I see the largest positive magnetization values ~10 A/m. Near the center of KEJ crater, there is a N-S trend of positive magnetization that can be correlated with the different 2-D lines. The magnetization values decrease and become negative as I move away from the inner crater toward the outer crater in a W-E trend.

The inversion results provided the starting point for the 3 different forward models that were used: polarity reversal (Fig. 6A), structural boundary (Fig. 6B), and lithological changes (Fig. 6C). The magnetization values were changed to provide a better fit between the observed magnetic anomaly and the forward model's predicted magnetic anomaly. Based on average RMSE, the polarity model best represented the observed magnetic anomaly (356 nT), followed by the structural boundary (773 nT), with the lithological model having the most error (1052 nT).

The magnetic source thickness and magnetization distribution was taken from the final forward model results and used to create my interpretation of the magnetic source below KEJ (Fig. 7C).

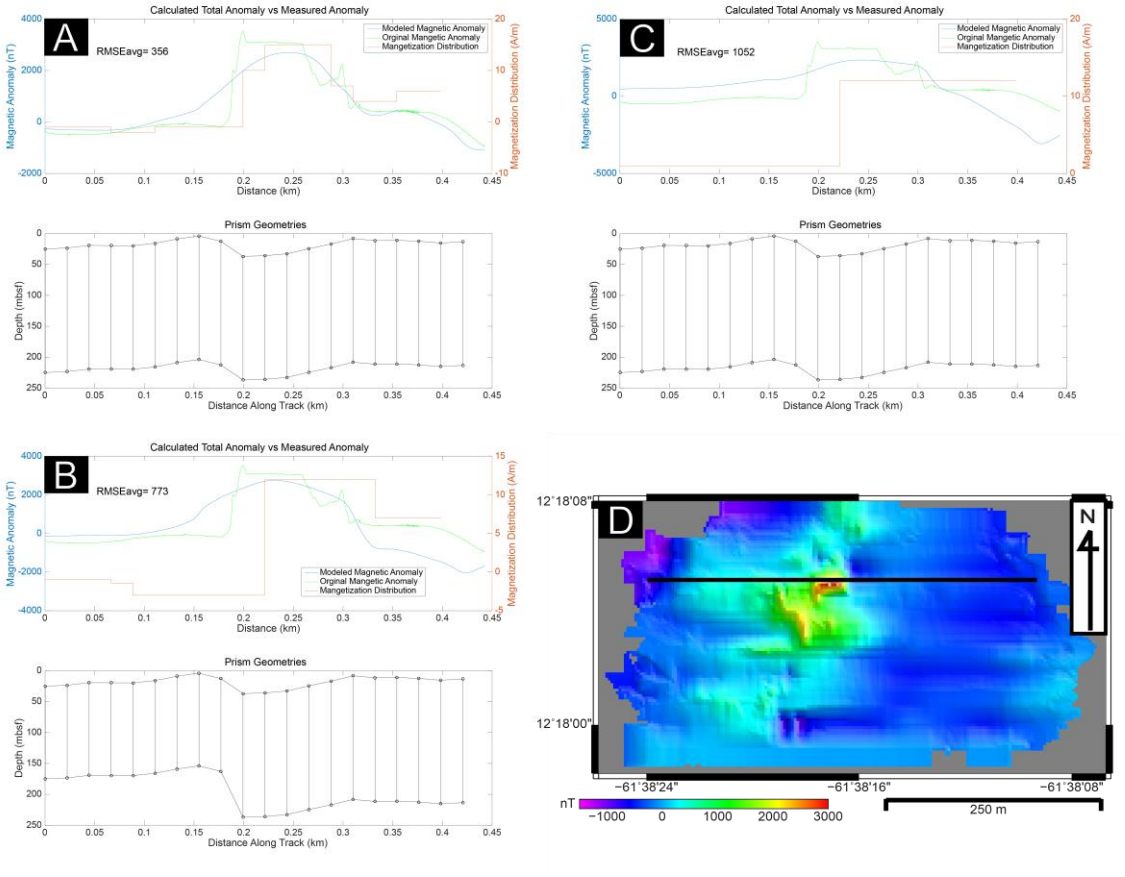

Figure 6. Magnetic Forward Models. Diagrams displaying the 3 different magnetic forward models that were used to investigate the source of the dichotomy in the magnetization distribution and magnetic anomaly signatures in the inner crater. (A) Polarity reversal model, average RMSE value of 356 nT. (B) Structural boundary model, average RMSE value of 773 nT. (C) Lithological model, average RMSE value 1052 nT. (D) Total magnetic field intensity map of the inner crater. Black line on the magnetic grid represents the magnetic survey line that these anomalies originate from.

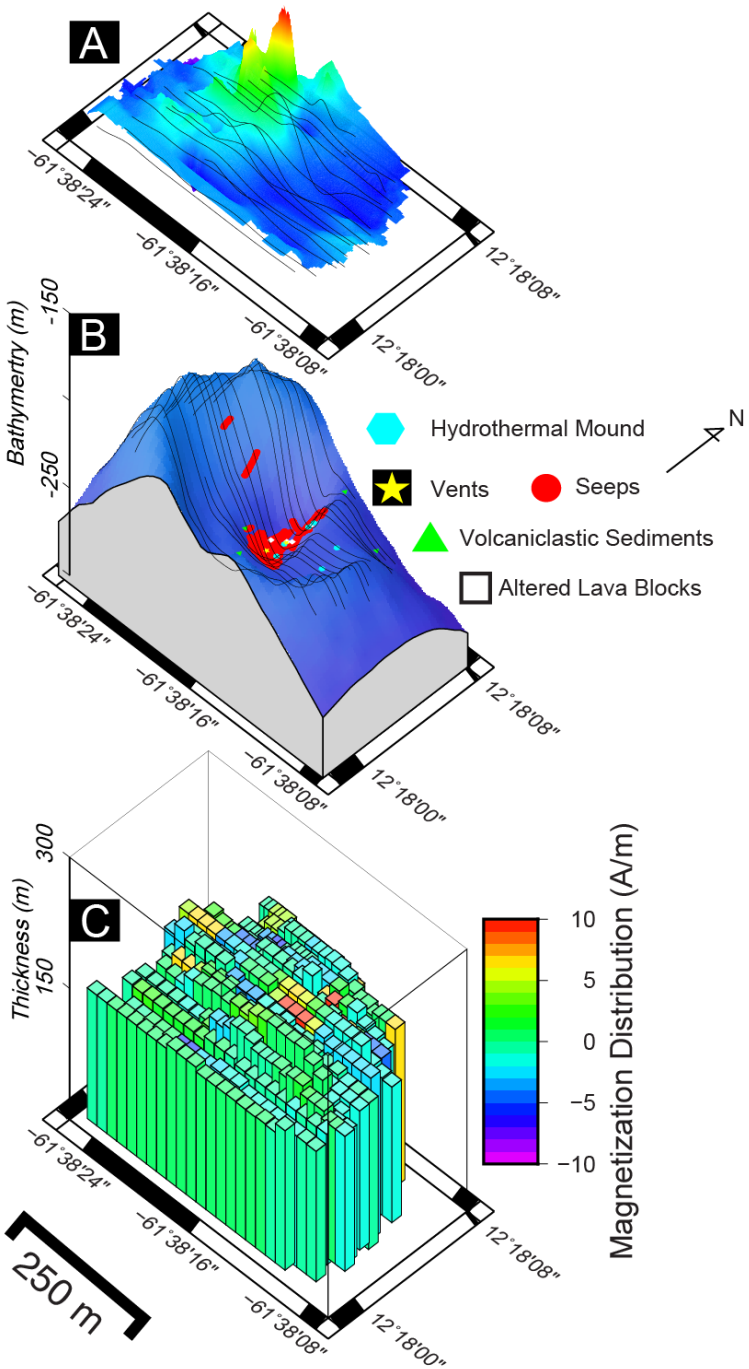

Figure 7. Magnetic Inversion and Forward Results. Magnetic inversion and forward modeling results: (A) Displays corrected magnetic anomaly grid, with magnetization distribution values of the 18 different track lines plotting on top for comparison. (B) Bathymetry of Kick 'em Jenny crater with key geologic features labeled and plotted. (C) Forward prism model with thickness of magnetic source layer under Kick 'em Jenny crater. Color represents magnetization distribution given to the different prisms.

4.4 Thin Section Analyses

Thin sections, NA054-004 and NA054-007, were added to the three other thin sections that were made from samples collected in the September 2013 E/V Nautilus cruise. The samples from 2013 were collected from the toe of the landslide, whereas the samples from 2014 were collected from the toe and near a contact between volcanic rock and lithified carbonate rock.

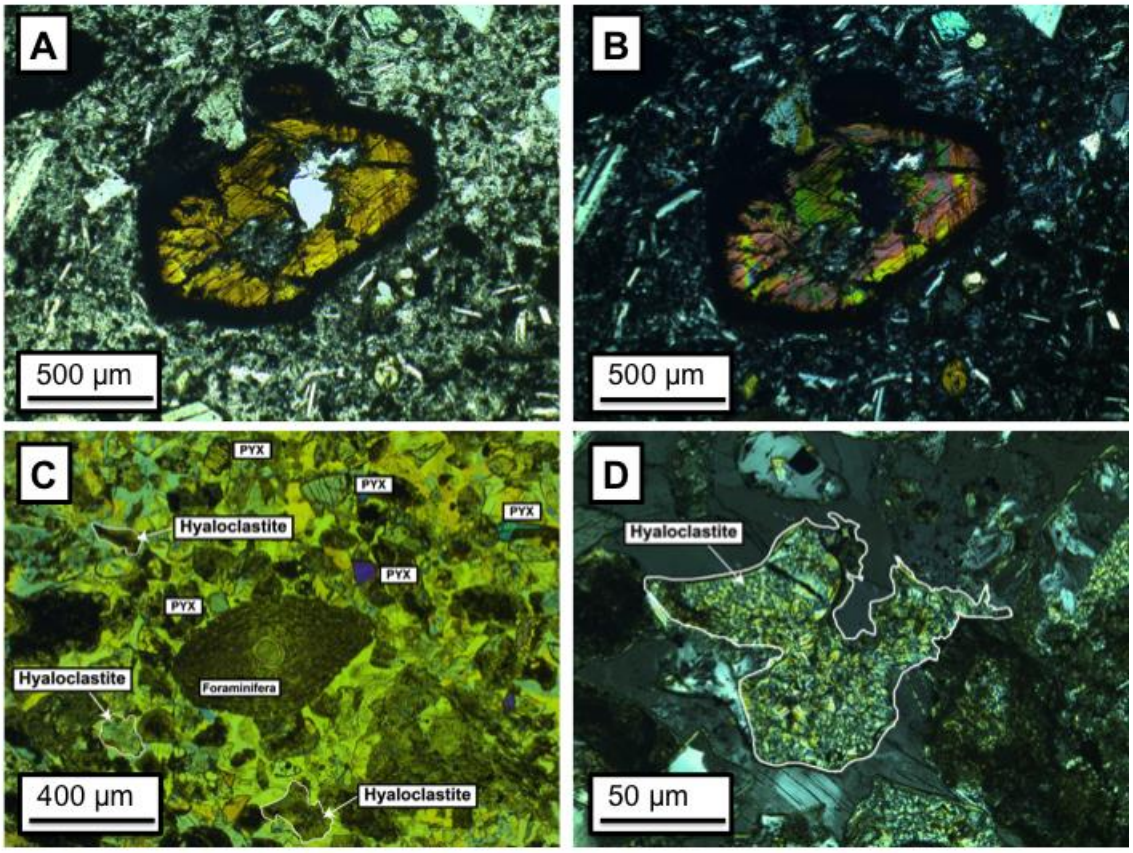

Figure 8. Thin Section Evidence for Volcanic Eruption. Four rock thin sections are shown to provide evidence for past rate of magma ascension, eruption depth and style. (A and B) are from sample NA054-004, (C and D) is from sample NA054-007, and both samples were collected from the toe at a depth of ca. 2200 m. (A) Amphibole phenocryst from sample NA054-004 in plain polarized light, and (B) Same amphibole phenocryst,

but in cross-polarized light. (C) Pyroclastic breccia that contains hyaloclastites. (D) 10x zoom in of a single round and highly fractured hyaloclastite.

Sample NA054-004, has amphibole breakdown rims present on the rims of the phenocryst (Fig. 8A and 8B). The grain displayed has a 90 micron thick breakdown rim, and the other amphibole grains have smaller or non-existent rims.

Sample NA054-007, hyaloclastites are seen in a pyroclastic breccia (Fig. 8C and 8D). Hyaloclastites form when basaltic lava erupted at water depths and the lava reacts with the water (Honorez and Kirst, 1975; Smith and Batiza, 1989). They are composed of super-cooled magma that turns into glass, which forms from the stress produced by super-cooling magma with water and not forming any lava flow (Carlisle, 1963; Honnorez, 1961; Nayudu, 1962).

5. DISCUSSION

5.1 Sediment Transportation Regime and the Nature of Landslides at KEJ

KEJ volcano's seafloor morphology exhibits a complex relationship between different submarine sedimentological activities: development of submarine channels and canyons (Fig. 2B) and the multi-generation of landslides (Fig. 4A), which play a major role in controlling sediment transportation regimes around an active submarine volcano. Volcanoes evolve over time, including permanently subaqueous volcanoes, represented by Lō'ihi in Hawaii and numerous other seamounts (Fornari et al. 1988; Malahoff and Woollard, 1968) and volcanoes that experienced both subaerial and submarine environments, represented by the Canary Islands (Krastel et al. 2001; Watts and Masson, 1995) and KEJ, have been known to be closely related to vigorous sediment transportation regimes by weathering and erosion processes of the volcanoes (Fornari et al. 1988; Malahoff, 1987; Watts and Masson, 1995). However, despite such pronounced observations on the well-evolved submarine canyons and channels in the vicinity of submarine portion of the volcanoes, mechanisms that formed these seafloor morphological features involving the weathering and erosion processes of the volcanoes and their roles in global sediment cycle and transportation systems have rarely been discussed to date.

Understanding the origins of the seafloor morphological features can provide an important first step to advance our understanding of the sediment transportation regime hosted by submarine volcanoes. Overall, contrasting features in the seafloor morphology

are observed at and in the vicinity of KEJ, i.e. the smooth flank of KEJ's cone and landslide surface just below the cone to the Grenada Basin (Fig. 2A), and a well-developed shelf platform composed with submarine canyons and channels (Fig. 2B). The formation scenarios of submarine canyons on the flanks of ocean islands depends on how a volcanoes experiences subaerial and submarine environments, i.e. whether the initiation of these sediment transportation systems has taken place by subaerial weathering and erosion of rocks or by sediment instability at submarine slopes (e.g. Moore et al. 1989; Krastel et al. 2001). To determine KEJ's canyon and channel formation scenarios, I first investigate whether the weathering and erosion started subaerially by assessing whether subsidence occurred or not. In the best proximal case, a subsidence rate of 0.4m/kyr is observed from the northern islands of Guadeloupe, which is a part of the same volcanic island arc chain (Leclerc et al. 2014). Although KEJ is located within the same island arc, this subsidence rate may not be directly applicable to KEJ because: (1) this subsidence rate at Guadeloupe is related to the Les Saintes fault system (Leclerc et al. 2014), and I do not see any connectivity of the Les Saintes fault system from Guadeloupe to Grenada; (2) even the seismic evidences, which are from the closest geographical locations that are attributed to any fault systems that could induce subsidence at KEJ, are located 17 km downslope from KEJ volcano, suggesting there is no subsidence occurring in the Grenada Basin (e.g. Aitken et al. 2011). Closer to KEJ, there is a mapped fault scarp near the crater (Sigurdsson and Shepherd, 1974), and the epicenters of the 2001 volcanic earthquakes appear to closely associate with this fault scarp, rather than with the volcanic activities of KEJ (Lindsay et al. 2005). However, it

has been debated whether this fault scarp is still active, inactive, or dormant, and assessing denser focal mechanism data is needed to determine if the source of these earthquakes are tectonic or volcanic related (e.g. Lindsay et al. 2005). Hence, I propose that there is no active subsidence occurring at KEJ; rather, the transition from a subaerial to submarine volcano has been attributed to instantaneous volcanic eruption and subsequent landslide events, supporting a scenario that Dondin et al. (2012) numerical simulations have predicted.

Without subsidence, these KEJ's submarine canyons have likely been formed from shallow, sediment-laden shelf currents, which pile up sediments on the island shelves, causing additional loads in the area, resulting in the gravity flows that erode the shelf platform. Erosion of the shelf platform is easy due to the biogenic and volcaniclastic source of sediments that cover the flanks near KEJ (Schmincke et al. 1995; Schmincke and Sumita, 1998). The evolution of KEJ began as a subaerial island like the Canary Islands, and could include the weathering and erosion that might have started on the KEJ volcanic cone; but soon volcanic activities altered the entire volcanic system to a subaqueous environment, where any sediment erosion and weathering features with subaerial origins were likely overprinted by both vigorous volcanic eruption events as well as other submarine sediment transport regimes.

Multiple generations of submarine landslides observed at KEJ flank indicate that a volumetrically significant sediment transport regime has taken place in addition to the submarine canyons and channel systems. To further understand this regime around an active submarine volcano in time and space, detailed morphological mapping of the

observations from bathymetry is undertaken (Fig. 2B). From seafloor morphological observations, it is clear that the landslide exhibits a crosscutting relationship, which that the formation of canyons and channels predates the landslides (Fig. 2A). This is because the depth of the canyon toe between the slopes around KEJ is deeper than at the toe of the landslide. Over longer periods of time, canyons and channels have played a major role in sediment transportation system around KEJ.

Our observations on morphology on the KEJ flank and landslide areas using both shipboard and high-resolution, near-bottom bathymetry maps (Fig. 2 and 5) revealed that three generations of landslides have occurred in KEJ vicinity (Fig. 4). The foundation of the current KEJ's flank structure is the deposit of the first-generation landslide (Fig. 4B). However, little is known about this landslide except it's area, 67 km^2 and extent, 17 km, which have been calculated from bathymetric data (Lindsay et al. 2005). Based on other landslide events in the Lesser Antilles, specifically events at Montagne Pelée, Martinique, it appears that landslides with such large areas covered, ca. 65 km^2, and long extent, ca. 17 km, form when there was a sector collapse of the volcano (Boudon et al. 2007; Dondin et al. 2012; Le Friant et al. 2003), indicating that it is possible that KEJ has undergone two sector collapses.

The second-generation landslide (Fig. 4C) was the primary focus for our survey because it is the landslide, induced by a volcanic event, which shaped the current edifice. The sampling and near-bottom observations that were collected are because I were able to groundtruth all of our observations that are seen in our bathymetric data. The columnar basalt (Fig. 5D), weighted an estimated ca. 144 tons in water, with a velocity

range of 2 – 30 m/s during the relocation due to the landslide from the caldera to the present location, 6 km laterally and 1.5 km vertically away (Fig. 2A), in 3.4- 51.5 minutes. The two cooling patterns, highly fractured (Fig. 5C) and columnar basalt (Fig. 5D), are unique cooling patterns of volcanic material that are seen at KEJ's crater. The presence of these volcanic rocks (Fig.5 C, D) in the second-generation landslide deposit allow us to propose that the transportation of the volcanic material was related to the sector collapse of KEJ (Dondin et al. 2012), which exhumed the cooled volcanic crater material from the subsurface of the crater, and the resulting landslide event, which moved the volcanic material from the crater to the survey area (Fig.5A).

The third generation landslide is difficult to identify as Dondin et al. (2012) only interpreted the central deposit to be apart of the third generation of landslides. Our new seafloor map revealed that the third generation is composed of a deposited located on the right, central, and left side of the previous landslide. By comparing the roundness of the lobe of a landslide deposit, a proxy of landslide timing (e.g. Mitchell et al., 2000; Cannat et al. 2013), I identified the location and distribution of the third generation landslide. I observed that the third generation has a round lobe, ca. 25° (Fig. 4D), and the second-generation has a steeper lobe, ca. 40° (Fig. 4C). The volume displaced by the third generation landslide is minimal compared to the first and second-generation slides, which displaced 227 and 15 times more material, respectively; yet it indicates the sediment transport regime by landslide has taken place multiple times. Within a short time period, both a submarine landslide and gravity flow event can occur instantaneously. The amount of material transported during a landslide event is,

however, vastly different between these two sediment transportation regimes at KEJ: the landslides can move ca. 4-67 km^3, a factor of 40-600 times more material than a single canyon could transport per an event of gravity flow.

The origin of these landslides at KEJ can be attributed to multiple different sources: volcanic activity, earthquakes, or underconsolidation (Masson et al. 2006; Wiemer et al. 2014). As previously discussed, the volcanic activities at KEJ have been a major cause of modifying the morphology of the volcano itself and seafloor, and monitoring when they occur is an important and challenging task. The earthquake seismicity monitoring system around KEJ's geographic area may be the most closely and intensively monitored submarine volcano anywhere in the world (Lindsay et al. 2005), with 50 seismic stations positioned in the Eastern Caribbean, and the closest station being 3 km to the east of the summit. There are two different types of seismicity activity recorded by these seismograph stations: (1) Volcanic related seismicity; and (2) earthquakes associated with large-scale tectonic movements. Distinguishing between the two sources is accomplished by observing the difference between the T-phase on the seismograph. A T-phase is a low-frequency acoustic wave generated during eruption events (Shepherd and Robson, 1967). The differences between T-phases generated by long-period volcanic earthquakes and earthquake generated by tectonic movements are evident in the time and frequency domain (Lindsay et al. 2005). In the time domain, the volcanic earthquakes T-phase last for 4-5 minutes, while the earthquakes themselves last 20-30 seconds (Lindsay et al. 2005). In the frequency domain, volcanic earthquakes will have higher frequencies in the .7 Hz to 10 Hz, whereas the earthquakes will have

frequencies mainly at 10 Hz or greater (Lindsay et al. 2005). This distinction is what has allowed for the interpretation that the seismic activity is primarily related to volcanic activity at KEJ. Additionally, underconsolidation is known to have cause landslides due to increased pore pressure on the underconsolidated sediments (Masson et al. 2005), and chemical alteration of existing rock (Mizota and Van Reeuwijk, 1989; Tucker, 2009). The alteration of volcanic rock to clay material is known to be a source of landslides due to the clay's low shear strength and friction coefficient (Leroueil and Hight, 2003; Wiemer et al. 2014). Carey et al. (2014) and Koshinsky et al. (2007) obtained visual observations of cold seeps on KEJ's landslide, which can be associated with larger amounts of clay present, due to the breakdown of volcanic material into clay material (Mizota and Van Reeuwijk, 1989; Tucker, 2009).

5.2 Pre-2014 Eruption at Kick 'em Jenny: In Situ Volcanic Activity

KEJ the only active volcano in the Lesser Antilles island arc with approximately 80 years of observable eruption cycles (Devas, 1974; Lindsay et al. 2005; McClelland et al. 1990; McClelland et al. 1989; Molard, 1947; Robertson et al. 2015; Shepherd, 1988; Shepherd and Robson, 1967; Sigurdsson, 1989). Indeed, KEJ erupted nine months after our cruise NA054, and there has yet to be a study on the most recent eruption. Toward understanding the volcanic eruption cycle and environmental impact, our near-bottom observations provide invaluable information. KEJ is a rare case study because there is a clear time scale between two different eruptions, 2001 to 2015, where I can observe the geologic process that occurred during this time. Normally, when other science teams

dive onto submarine volcanoes, i.e. Piton del la Fournaise volcano, the data gathered is not a dataset that provides insight into an active volcanic eruption and environmental impact.

Characterizing subsurface magmatic activities including: dimensions of a magma chamber, magma conduits, and diking system that yield eruption events, is a challenging problem in geophysics. The subtle density contrasts, and dimensions of the volcano cones often preclude us from successfully conducting inactive seismic source surveys due to the wavelength resolution issues, let alone the non-unique solutions in gravity and seismic monitoring surveys, in the submarine context particularly. Nevertheless, in recent years, high-resolution magnetic anomaly data has been used to provide constraints to detect and study hydrothermal activity, study the hydrothermal activities affect on the magnetization value of the basalt and andesite hosted rocks, and to investigate the magnetic structure of a slow spreading ridge (Fujii et al. 2015; Honsho et al. 2009; Szitkar et al. 2015a; Szitkar et al. 2015b), advancing our understanding of the subsurface characterizations of submarine volcanic systems. Total field magnetic anomaly data has been used to study active volcanoes to understand the current magmatic processes currently occurring, because of the passive nature of magnetic data. High magnetic anomalies can arise in TMI data, after IGRF and diurnal variations corrections, from various different scenarios: geomagnetic polarity reversal (Vine and Matthews, 1963), represented by West Blanco Scarp, northeast Pacific (Tivey et al. 1998); tectonic juxtaposition of rock units with differing magnetic properties (Grauch et al. 2006), represented by San Ysidro Fault, New Mexico, USA (Grauch et al. 2006); and changes

in the local lithology (Vine and Matthews, 1963), represented by Piton del la Fournaise volcano, La Reunion Island, Indian Ocean (Lenat and Aubert, 1982) and Lō'ihi in Hawaii (Malahoff, 1987). Interpretation of magnetic data depends on the set of geological constraints, such as source locations, lithology, geometry, and age data, applied to the models. Having accurate constraints helps limit the number of models that can fit to the observed magnetic anomaly. Our detailed magnetic survey in the inner crater produced a magnetic anomaly high (~3000 nT) that corresponds to the area at the inner crater, and low magnetic intensities (~ -100 nT) on the eastern side of KEJ's crater (Fig. 6D). To investigate the magnetic source distribution, I conducted a magnetic inversion modeling that yielded a high magnetization distribution at the inner crater (~10 A/m) and low magnetization distribution on the eastern half of the crater (~ -3 A/m). To assess the origins of this dichotomy in magnetization distribution at KEJ crater, I investigate the following scenarios: polarity reversal (Fig. 6A), structural boundary (Fig. 6B), and lithological changes (Fig. 6C).

Ocean crust preserves ambient magnetic field as the crust is formed, which has provided significant evidence to support seafloor spreading at mid ocean ridges, in turn, plate tectonics (Vine and Matthews, 1963). Although seafloor spreading magnetic anomalies are commonly known to produce the most pronounced magnetic anomaly signatures in world's ocean basins (e.g. Vine and Matthews, 1963), the scale of magnetic anomalies associated with the caldera of a submarine active volcano can be much smaller and shorter, in space and time, respectively. Moreover, KEJ is an active submarine volcano that has been erupting every decade, with the oldest known age

constraint being 43.5 kyr BP, based on radiocarbon dating (Dondin et al .2017), and the formation and evolution of KEJ is happening all with in the Brunches Chron, which began 780 kyr BP. This allows us to omit a polarity reversal as the source of the dichotomy in magnetization distribution I observe in KEJ Caldera.

Faults are ubiquitously observed in the caldera of active volcanoes (Smith and Baily, 1968) as a consequence of: magma chamber inflation or deflation (Walter and Troll, 2000), both represented by Darwin Caldera, Galápagos Island (McBirney and Williams, 1969); inward-slumping of the caldera (Walter and Troll, 2000); and uplift of the caldera floor (Walter and Troll, 2000), represented by Ischia Caldera, Italy (Tibaldi and Vezzoli, 1998). There is video evidence of faults in the inner crater (Carey et al. 2016), with another fault scarp, 50 m of vertical offset, 1 km east of KEJ crater (Lindsay, 2005; Sigurdsson and Shepherd, 1974). I have considered the possibility of structural influence that caused the observed linear trend in the magnetic anomaly grid (Fig. 6D); observed faults in the inner crater controlling the fluid venting (Carey et al. 2016). There is a trend that runs NNE-SSW through the center of KEJ crater (Fig. 6D), on the eastern half of the crater is lower magnetic anomaly values (-500 nT – 500 nT), whereas on the western side has the higher magnetic anomaly values (-500 nT – 3000 nT). I interpreted this trend as being a potential fault running through the crater, and uplifting the eastern half of the crater, giving it less magnetic source.50 m offset is used because that is the offset that is seen at fault scarp near KEJ crater (Lindsay, 2005; Sigurdsson and Shepherd, 1974). I take the fault into account by moving the bottom of our prisms' magnetic source, in the model 50 m up, on the eastern side of the crater (Fig. 6B). I

obtained a 773 nT RMSE value, which is a high value indicating lower agreement between the observed magnetic anomaly and forward-modeled magnetic anomaly. Taking into consideration that faulting is seen within (Carey et al. 2016) and near (Lindsay et al. 2005) KEJ caldera, and faulting within volcanic craters is a ubiquitous feature (Smith and Baily, 1968), together with our modeling results, I consider 50 m fault in the magnetic source layer to be an origin of the dichotomy of magnetization values observed at KEJ Caldera (Fig. 7C).

Magnetic anomalies can arise from lithology contrast with different types and amounts of iron bearing materials (Macdonald and Abbott, 1970). Lithological boundaries in the form of a dike complex, has been shown to cause magnetic anomaly highs at other submarine volcanoes in Hawaii (Malahoff and Wollard, 1968) and on the La Réunion island (Lenat and Aubert, 1982). These dike complexes are characterized by higher density and higher magnetization than the surrounding lava, due to the higher density because feeder dikes have less vesiculation (Macdonald and Abbott, 1970), allowing for more magnetic rich material to be in the dikes. A potential dike swarm is modeled by thickening the prisms in the forward model (Fig. 6C) where there is the magnetic anomaly high in the inner crater (Fig. 6D). A 1072 nT RMSE value, which is a high value indicating lower agreement between the observed magnetic anomaly and forward-modeled magnetic anomaly. Whether or not these dikes contribute to create the 50m fault like structure predicted by our modeling remains uncertain. However, given a wholesale operation mechanism of an active volcano is drive by dike swarms from a

magma chamber to the shallow subsurface of its caldera, I propose that on-going melt transport by dikes below the western half of the inner crater is the best candidate to explain the dichotomy in magnetization distribution.

Furthermore, in active volcanic and magmatic systems, hydrothermal activity has been shown to demagnetize the iron bearing rocks (Szitkar et al. 2015a; Tivey and Johnson, 2002; Tivey and Johnson, 2001), with the rate of demagnetization related to the temperature of the fluid (Tivey et al. 2014). When surface geology is plotted on top of the magnetic anomaly, a spatial correlation is highlighted between the low magnetization area and low-temperature (55°C - 180°C, Carey et al. 2016) hydrothermal seeps and vents in the KEJ caldera, similar to low-temperature (~60°C) hydrothermal vent field at Tyrrhenian Sea, Italy (Szitkar et al. 2015b). The low temperature hydrothermal alteration provides an additional explanation for the presence of a magnetic anomaly low in the eastern half of the inner crater, enhancing the dichotomy of the magnetization distribution.

I determined that it is likely some combination of both a structural and lithological influence, which yields the optimal model to represent the observed magnetic anomalies. With additional support from visual evidence of faults in the inner crater (Carey et al. 2016), and hydrothermal activity (55°C - 180°C) (Carey et al. 2016), surrounding the magnetic anomaly high. The vents at KEJ have high temperatures fluids at their sites, 180°C (Carey et al. 2016), whereas the seeps have the lower temperatures, 55°C, and the magnetic anomaly highs occur where there are only observed seeps, no vents. The low temperature hydrothermal alteration provides an additional explanation

for the presence of a magnetic anomaly high because the demagnetization does not occur as readily in low temperature environments. Dike complexes have known to cause magnetic anomaly highs within craters of volcanoes in other locations (i.e. Hawaii (Malahoff and Wollard, 1968) and on the La Réunion island (Lenat and Aubert, 1982)). Pairing the dike complex with low temperature hydrothermal alteration, I propose these two lithological sources are a source of the dichotomy of magnetization values I observe at KEJ Caldera. I propose the thickness of the magnetic source layer is about 150 m thick over the eastern half of KEJ caldera, and 200 m over the western half of the caldera (Fig. 7C).

Our petrographical and petrological observations of in situ rock samples collected during the ROV survey provided evidence of previous KEJ volcanic events, which allows us to deduce a possible next eruptions and associated volcanic processes scenario. At a volcano, the magma ascends from the magma chamber to the surface of the volcano by a magma conduit. I are able infer the rate at which the magma rose though the magma conduit based on the thickness of the breakdown rim observed on amphibole grains in the volcanic rocks (Devine et al. 1998; Devine and Sigurdsson, 1995). To analyze the breakdown rims on the amphibole grains at KEJ, Rock sample NA054-004 was collected from the toe of KEJ, ca. 2000 mbsl. After examining sample NA054-004 in thin sections, it is observed that there were more amphibole grains that lacked a breakdown rim; which is consistent with previous studies (Devine and Sigurdsson, 1995), suggesting that KEJ's magma ascended rapidly through the magma chamber. An assumption that is made with a quickly rising magma is that the eruption is

likely explosive since it moved through the magma chamber quickly. KEJ's distribution of breakdown rims is similar to another Lesser Antilles volcano that recently erupted, the Soufriere Hills Volcano, which is documented as an explosive eruption (Sparks et al. 2002; Voight et al. 2002). When KEJ erupted, it created formed highly fractured hyaloclastites (Fig. 8C and 8D). (Honnez and Kirst, 1973; and Smith and Balt, 1989) have shown that this cooling pattern of the hyaloclastites form from explosive interaction between water and lava, and explosives eruptions can only occur in shallow water depth. Taking into consideration the location at which these rocks were collected and the present day location of KEJ's crater (Fig. 2), it shows a landslide transported this material 5 km laterally and 1.5 km vertically. This material is found in the second-generation landslide area, and this is the landslide that was numerical predicted to cause a tsunami comparable to the 1998 Papa New Guinea Tsunami (Heinrich et al. 2001; Tappin et al. 2008). When KEJ did erupt in this shallow water depth, it was an explosive eruption. Sample NA054-007, displays unique hyaloclastites because they are highly fractured and have concave edges (Fig, 8C). In order to have this cooling pattern of the hyaloclastites, the interaction between the lava and water must be explosive. Explosive eruptions only occur in shallow water depth because there is less pressure exerted from the above water column. Rock sample NA054-007 is found at a depth of ca. 2200 m, and no explosive eruptions can occur at such depths.

I propose the following cyclic evolution scenario of KEJ throughout eruption events to inter-eruption periods. By combining the seafloor morphology observations, integrating high-resolution bathymetry maps, ROV visuals, and rock samples from the

wholesale KEJ, and subsurface characterization with high-resolution near-bottom magnetic survey of KEJ crater and inner crater. KEJ originally formed from arc volcanism from the subducting North and South American plates underneath the Caribbean plate (Fig. 9A), and our premise here is that KEJ volcanism has been operated by the archetypical active volcano operation regime (Melnik and Sparks, 1999) that consists of magma chamber, magma conduit to the shallow subsurface associating with a series of diking, then eruption. Based on the lack of breakdown rims in the volcanic material (Fig. 8A and 8B), the magma would rise quickly from the magma chamber through the conduits (Fig. 9B). This magma was quenched as a series of approximately 200-m thick dikes right below the inner crater, atleast during pre-2015 eruption period, based on our magnetic analyses. Then, the magma erupted at shallow water depth suggested by the presence of highly fractured hyaloclastites in the volcanic breccia rock samples (Fig. 8). When erupted, the eruption style was explosive (Fig. 9C), as our highly fractured hyaloclastites have shown (Fig. 8C and 8D). This eruption then triggered a landslide and deposited material downslope from the crater (Fig. 9D). Lastly, submarine canyons began to form (Fig. 9E) from in situ gravity flows, waiting for the next eruption event. This is the likely evolutionary scenario that KEJ cycles through before, during, and after a volcanic eruption.

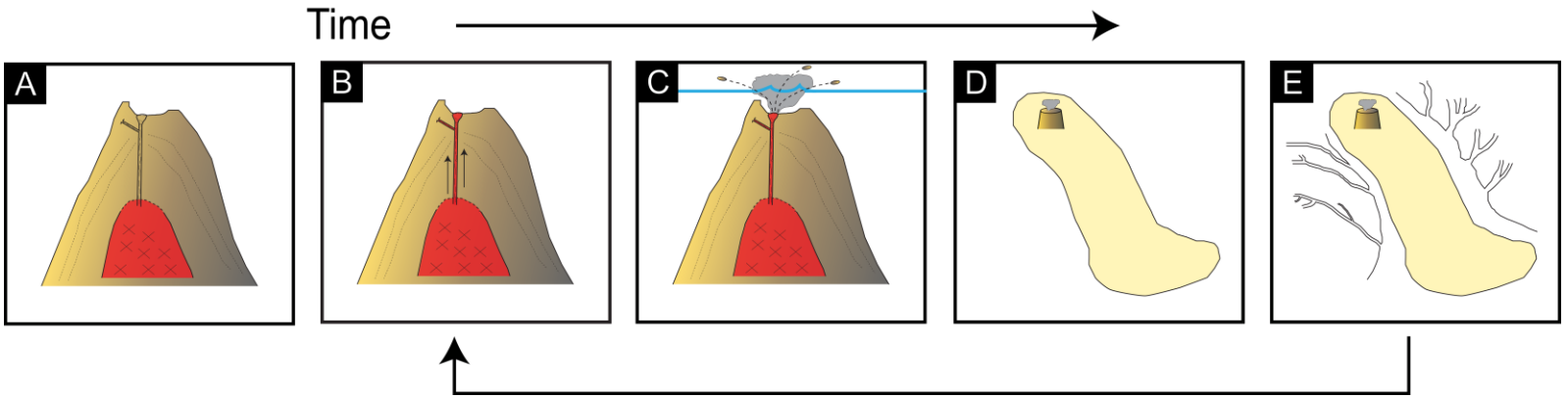

Figure 9. KEJ Cyclic Evolution Scenarios. Diagrams showing the volcanic evolutionary path of KEJ. (A) Scenario in which KEJ volcanism occurs, dike complexes feed the magma to the surface location of the inner crater. (B) The magma rises quickly from the magma chamber through the dikes to the surface. (C) KEJ was in a shallow water depth and erupted explosively in the past. (D) After the eruption, a resulting landslide changes the seafloor morphology. (E) Submarine canyons and channels form from in situ submarine gravity flows. When the step reaches step E, the process starts over and begins again at step (B). However, in step (C), the depth for eruption can potentially change, depending on the failure style, and can be deeper in the water column.

6. CONCLUSIONS

The conclusions from this study are:

(1) There is no active subsidence occurring at KEJ; rather, the transition from a subaerial to submarine volcano at KEJ has been induced by a volcanic eruption and subsequent landslide;

(2) Over longer periods of time, canyons and channels have played a major role in sediment transportation system around KEJ;

(3) The landslides at KEJ moved 40-600 times more material during one single instantaneous event than that a single canyon could transport;

(4) There is a magnetic anomaly high at the inner crater at KEJ, which has both lithological (dike complex) and structural (fault) sources of the variety of magnetization values I observe at KEJ Caldera;

(5) Rock samples from the second-generation landslide deposit indicate that KEJ volcanism had a history of shallow water depth and explosive eruptions.

These conclusions allowed us to propose an eruption model for the second-generation landslide and a cyclic evolution scenario for KEJ volcanism.

REFERENCES

Aitken, T., Mann, P., Escalona, A., Christeson, G.L., 2011. Evolution of the Grenada and Tobago basins and implications for arc migration. Mar. Pet. Geol. 28, 235–258. doi:10.1016/j.marpetgeo.2009.10.003

Assier-Rzadkieaicz, S., Heinrich, P., Sabatier, P.C., Savoye, B., Bourillet, J.F., 2000. Numerical modelling of a landslide-generated tsunami: The 1979 Nice event. Pure Appl. Geophys. 157, 1707–1727. doi:10.1007/PL00001057

Bell, K.L.C., Carey, S.N., Nomikou, P., Sigurdsson, H., Sakellariou, D., 2013. Submarine evidence of a debris avalanche deposit on the eastern slope of Santorini volcano, Greece. Tectonophysics 597–598, 147–160. doi:http://dx.doi.org/10.1016/j.tecto.2012.05.006

Bleeker, W., Ernst, R., 2006. Short-lived mantle generated magmatic events and their dyke swarms: the key unlocking Earth's paleogeographic record back to 2.6 Ga, Dyke swarms--time markers of crustal evolution. AA Balkema, Rotterdam, Netherlands.

Boudon, G., Le Friant, A., Komorowski, J.-C., Deplus, C., Semet, M.P., 2007. Volcano flank instability in the Lesser Antilles Arc: Diversity of scale, processes, and temporal recurrence. J. Geophys. Res. Solid Earth 112, 1–24. doi:10.1029/2006JB004674

Bryn, P., Berg, K., Forsberg, C.F., Solheim, A., Kvalstad, T.J., 2005. Explaining the Storegga Slide. Mar. Pet. Geol. 22, 11–19. doi:10.1016/j.marpetgeo.2004.12.003

Bullen, R.P., 1964. The Archaeology of Grenada, West Indies. University of Florida, Gainsville.

Cannat, M., Mangeney, A., Ondréas, H., Fouquet, Y., Normand, A., 2013. High-resolution bathymetry reveals contrasting landslide activity shaping the walls of the Mid-Atlantic Ridge axial valley. Geochemistry, Geophys. Geosystems 14, 996–1011. doi:10.1002/ggge.20056

Carey, S., Ballard, R., Bell, K.L.C., Bell, R.J., Connally, P., Dondin, F., Fuller, S., Gobin, J., Miloslavich, P., Phillips, B., Roman, C., Seibel, B., Siu, N., Smart, C., 2014. Cold seeps associated with a submarine debris avalanche deposit at Kick'em Jenny volcano, Grenada (Lesser Antilles). Deep Sea Res. Part I Oceanogr. Res. Pap. 93, 156–160. doi:http://dx.doi.org/10.1016/j.dsr.2014.08.002

Carey, S., Olsen, R., Bell, K.L.C., Ballard, R., Dondin, F., Roman, C., Smart, C., Lilley, M., Lupton, J., Seibel, B., Cornell, W., Moyer, C., 2016. Hydrothermal venting and mineralization in the crater of Kick'em Jenny submarine volcano, Grenada (Lesser Antilles). Geochemistry, Geophys. Geosystems 17, 1000–1019. doi:10.1002/2015GC006060

Clouard, V., Bonneville, A., 2001. How many Pacific hotspots are fed by deep-mantle plumes? Geology 29, 695–698.

Crisp, J.A., 1984. Rates of magma emplacement and volcanic output. J. Volcanol. Geotherm. Res. 20, 177–211. doi:http://dx.doi.org/10.1016/0377-0273(84)90039-8

Crozier, M.J., 1973. Techniques for the morphometric analysis of landslips. Zeitschrift für Geomorphol. 17, 78–101.

Cummins, P.R., 2007. The potential for giant tsunamigenic earthquakes in the northern Bay of Bengal. Nature 449, 75–78.

Day, S., Llanes, P., Silver, E., Hoffmann, G., Ward, S., Driscoll, N., 2015. Submarine landslide deposits of the historical lateral collapse of Ritter Island, Papua New Guinea. Mar. Pet. Geol. 67, 419–438. doi:http://dx.doi.org/10.1016/j.marpetgeo.2015.05.017

De Blasio, F.V., Engvik, L.E., Elverhøi, A., 2006. Sliding of outrunner blocks from submarine landslides. Geophys. Res. Lett. 33, 8–11. doi:10.1029/2005GL025165

Devas, R.P., 1974. A history of the island of Grenada. Carenage Press.

Devine, J.D., Rutherford, M.J., Gardner, J.E., 1998. Petrologic determination of ascent rates for the 1995–1997 Soufriere Hills Volcano andesitic magma. Geophys. Res. Lett. 25, 3673–3676. doi:10.1029/98GL00912

Devine, J.D., Sigurdsson, H., 1995. Petrology and eruption styles of Kick'em-Jenny submarine volcano, Lesser Antilles island arc. J. Volcanol. Geotherm. Res. 69, 35–58. doi:http://dx.doi.org/10.1016/0377-0273(95)00025-9

Dondin, F., Lebrun, J.-F., Kelfoun, K., Fournier, N., Randrianasolo, A., 2012. Sector collapse at Kick 'em Jenny submarine volcano (Lesser Antilles): numerical simulation and landslide behaviour. Bull. Volcanol. 74, 595–607. doi:10.1007/s00445-011-0554-0

Dondin, F.J.-Y., Heap, M.J., Robertson, R.E.A., Dorville, J.-F.M., Carey, S., 2017. Flank instability assessment at Kick-'em-Jenny submarine volcano (Grenada, Lesser Antilles): a multidisciplinary approach using experiments and modeling.

Bull. Volcanol. 79, 1–15. doi:10.1007/s00445-016-1090-8

Eldholm, O., Thomas, E., 1993. Environmental impact of volcanic margin formation. Earth Planet. Sci. Lett. 117, 319–329.

Fagents, S.A., Gregg, T.K.P., Lopes, R.M.C., 2013. Modeling volcanic processes: the physics and mathematics of volcanism. Cambridge University Press.

Fine, I. V., Rabinovich, A.B., Bornhold, B.D., Thomson, R.E., Kulikov, E.A., 2005. The Grand Banks landslide-generated tsunami of November 18, 1929: Preliminary analysis and numerical modeling. Mar. Geol. 215, 45–57. doi:10.1016/j.margeo.2004.11.007

Fornari, D.J., Garcia, M.O., Tyce, R.C., Gallo, D.G., 1988. Morphology and structure of Loihi Seamount on seabeam sonar mapping. J. Geophys. Res. 93, 15227–15238.

Fujii, M., Okino, K., Honsho, C., Dyment, J., Szitkar, F., Mochizuki, N., Asada, M., 2015. High-resolution magnetic signature of active hydrothermal systems in the back-arc spreading region of the southern Mariana Trough. J. Geophys. Res. Solid Earth 120, 2821–2837. doi:10.1002/2014JB011714

Grauch, V.J.S., Hudson, M.R., Minor, S. a., Caine, J.S., 2006. Sources of along-strike variation in magnetic anomalies related to intrasedimentary faults: a case study from the Rio Grande Rift, USA. Explor. Geophys. 37, 372–378. doi:10.1071/EG06372

Hayashi, J.N., Self, S., 1992. A comparison of pyroclastic flow and debris avalanche mobility. J. Geophys. Res. Solid Earth 97, 9063–9071. doi:10.1029/92JB00173

Haymon, R.M., Fornari, D.J., Von Damm, K.L., Lilley, M.D., Perfit, M.R., Edmond,

J.M., Shanks, W.C., Lutz, R.A., Grebmeier, J.M., Carbotte, S., others, 1993. Volcanic eruption of the mid-ocean ridge along the East Pacific Rise crest at 9 45--52′ N: Direct submersible observations of seafloor phenomena associated with an eruption event in April, 1991. Earth Planet. Sci. Lett. 119, 85–101.

Heinrich, P., Mangeney, A., Guibourg, S., Roche, R., Boudon, G., Cheminée, J., 1998. Simulation of water waves generated by a potential debris avalanche in Montserrat, Lesser Antilles. Geophys. Res. Lett. 25, 3697–3700. doi:10.1029/98GL01407

Heinrich, P., Piatanesi, A., Hébert, H., 2001. Numerical modelling of tsunami generation and propagation from submarine slumps: The 1998 Papua New Guinea event. Geophys. J. Int. 145, 97–111. doi:10.1046/j.1365-246x.2001.00336.x

Henderson, M., 2000. Gas leak may solve riddle of North Sea triangle. The Times of London.

Hillier, J.K., Watts, A.B., 2007. Global distribution of seamounts from ship-track bathymetry data. Geophys. Res. Lett. 34, 1–5. doi:10.1029/2007GL029874

Honnorez, J., Kirst, P., 1975. Submarine basaltic volcanism: Morphometric parameters for discriminating hyaloclastites from hyalotuffs. Bull. Volcanol. 39, 441–465. doi:10.1007/BF02597266

Honsho, C., Dyment, J., Tamaki, K., Ravilly, M., Horen, H., Gente, P., 2009. Magnetic structure of a slow spreading ridge segment: Insights from near-bottom magnetic measurements on board a submersible. J. Geophys. Res. Solid Earth 114, 1–25.

Horbitz, C.B., Lovholt, F., Pedersen, G., Masson, D.G., 2006. Mechanisms of tsunami generation by submarine landslides: a short review. Nor. Geol. Tidsskr. 86, 255–

264.

Jones, C.E., Jenkyns, H.C., 2001. Seawater strontium isotopes, oceanic anoxic events, and seafloor hydrothermal activity in the Jurassic and Cretaceous. Am. J. Sci. 301, 112–149.

Kay, R.W., Kay, S.M., 1993. Delamination and delamination magmatism. Tectonophysics 219, 177–189.

Koschinsky, A., Seifert, R., Knappe, A., Schmidt, K., Halbach, P., 2007. Hydrothermal fluid emanations from the submarine Kick'em Jenny volcano, Lesser Antilles island arc. Mar. Geol. 244, 129–141. doi:http://dx.doi.org/10.1016/j.margeo.2007.06.013

Krastel, S., Schmincke, H.-U., Jacobs, C.L., Rihm, R., Le Bas, T.P., Alibés, B., 2001. Submarine landslides around the Canary Islands. J. Geophys. Res. Solid Earth 106, 3977–3997.

Kvalstad, T.J., Nadim, F., Arbitz, C.B., others, 2001. Deepwater geohazards: geotechnical concerns and solutions, in: Offshore Technology Conference.

Larsen, H.C., Saunders, A.D., 1998. 41. Tectonism and volcanism at the southeast Greenland rifted margin: a record of plume impact and later continental rupture, in: Proceedings of the Ocean Drilling Program, Scientific Results. pp. 503–533.

Le Friant, A., Boudon, G., Deplus, C., Villemant, B., 2003. Large-scale flank collapse events during the activity of Montagne Pelée, Martinique, Lesser Antilles. J. Geophys. Res. Solid Earth 108, 1–15. doi:10.1029/2001JB001624

Leclerc, F., Feuillet, N., Cabioch, G., Deplus, C., Lebrun, J.F., Bazin, S., Beauducel, F., Boudon, G., Lefriant, A., Min, L. De, Melezan, D., 2014. The Holocene drowned

reef of Les Saintes plateau as witness of a long-term tectonic subsidence along the Lesser Antilles volcanic arc in Guadeloupe. Mar. Geol. 355, 115–135. doi:10.1016/j.margeo.2014.05.017

Lenat, J.F., Aubert, M., 1982. Structure of piton de la fournaise volcano (La Reunion island, Indian ocean) from magnetic investigations. An illustration of the analysis of magnetic data in a volcanic area. J. Volcanol. Geotherm. Res. 12, 361–392. doi:10.1016/0377-0273(82)90035-X

Leroueil, S., Hight, D.W., 2003. Behaviour and properties of natural soils and soft rocks. Characterisation Eng. Prop. Nat. soils 1, 29–254.

Lindsay, J.M., Shepherd, J.B., Wilson, D., 2005. Volcanic and Scientific Activity at Kick 'em Jenny Submarine Volcano 2001--2002: Implications for Volcanic Hazard in the Southern Grenadines, Lesser Antilles. Nat. Hazards 34, 1–24. doi:10.1007/s11069-004-1566-2

Locat, J., Lee, H.J., 2002. Submarine landslides: advances and challenges. Can. Geotech. J. 39, 193–212. doi:10.1139/t01-089

Macdonald, G.A., Abbott, A.T., Peterson, F.L., 1970. Volcanoes in the sea: Honolulu, University Press of Hawaii. University Press of Hawaii.

Machida, S., Ishii, T., 2003. Backarc volcanism along the en echelon seamounts: The Enpo seamount chain in the northern Izu-Ogasawara arc. Geochemistry, Geophys. Geosystems 4, 1–20. doi:10.1029/2003GC000554

Malahoff, A., 1987. Geology of the summit of Loihi submarine volcano, USGS. USGS.

Malahoff, A., Woollard, G.P., 1968. Magnetic and tectonic trends over the Hawaiian

Ridge. Crust Up. Mantle Pacific Area 241–276.

Marchant, J., 2000. Monsters of the deep [WWW Document]. New Sci.

Masson, D.G., 1996. Catastrophic collapse of the volcanic island of Hierro 15 ka ago and the history of landslides in the Canary Islands. Geology 24, 231–234.

Masson, D.G., Harbitz, C.B., Wynn, R.B., Pedersen, G., Løvholt, F., 2006. Submarine landslides: processes, triggers and hazard prediction. Philos. Trans. R. Soc. London A Math. Phys. Eng. Sci. 364, 2009–2039. doi:10.1098/rsta.2006.1810

Masson, D.G., Watts, A.B., Gee, M.J.R., Urgeles, R., Mitchell, N.C., Le Bas, T.P., Canals, M., 2002. Slope failures on the flanks of the western Canary Islands. Earth-Science Rev. 57, 1–35.

McAdoo, B.G., Moore, A., Baumwoll, J., 2009. Indigenous knowledge and the near field population response during the 2007 Solomon Islands tsunami. Nat. Hazards 48, 73–82.

McBirney, A.R., Williams, H., 1969. Geology and petrology of the Galapagos Islands. Geol. Soc. Am. Mem. 118, 1–197.

McClelland, L., 1989. Global volcanism 1975-1985: the first decade of reports from the Smithsonian Institution's Scientific Event Alert Network (SEAN). Prentice Hall.

McClelland, L., Romanak, K., Stein, T.C., Kivimaki, K., 1990. Kick'em Jenny. Smithson. Inst. Bull. Glob. Volcanism Netw. 15, 2.

Melnik, O., Sparks, R.S.J., 1999. Non-linear dynamics of lava extrusion. Nature 402, 37–41.

Mitchell, N., Tivey, M., 2000. Slopes of mid-ocean ridge fault scarps from submersible

observations observations and implications for interpreting geology from. Earth Planet. Sci. Lett. 183, 543–555.

Mizota, C., Van Reeuwijk, L.P., others, 1989. Clay mineralogy and chemistry of soils formed in volcanic material in diverse climatic regions., ISM Monograph. University of Wageningen, Wageningen, The Netherlands.

Molard, P., 1947. Tremblements de terre des Petites Antilles et manifestations actuelles du volcanisme de l'archipel (1936 à 1943). Ann. Géophys. 3, 113–140.

Moore, J.G., Clague, D. a., Holcomb, R.T., Lipman, P.W., Normark, W.R., Torresan, M.E., 1989. Prodigious submarine landslides on the Hawaiian Ridge. J. Geophys. Res. 94, 17465–17484. doi:10.1029/JB094iB12p17465

Moore, J.G., Normark, W.R., Holcomb, R.T., 1994. Giant Hawaiian Landslides. Annu. Rev. Earth Planet. Sci. 22, 119–144. doi:10.1146/annurev.ea.22.050194.001003

Moore, J.G., Schilling, J.-G., 1973. Vesicles, water, and sulfur in Reykjanes Ridge basalts. Contrib. to Mineral. Petrol. 41, 105–118. doi:10.1007/BF00375036

Parker, R.L., Huestis, S.P., 1974. The inversion of magnetic anomalies in the presence of topography. J. Geophys. Res. 79, 1587–1593. doi:10.1029/JB079i011p01587

Polet, J., Kanamori, H., 2000. Shallow subduction zone earthquakes and their tsunamigenic potential. Geophys. J. Int. 142, 684–702.

Randolph, M.F., White, D.J., 2012. Interaction forces between pipelines and submarine slides—A geotechnical viewpoint. Ocean Eng. 48, 32–37.

Roberts, N.J., McKillop, R.J., Lawrence, M.S., Psutka, J.F., Clague, J.J., Brideau, M.-A., Ward, B.C., 2013. Impacts of the 2007 Landslide-Generated Tsunami in Chehalis

Lake, Canada, in: Margottini, C., Canuti, P., Sassa, K. (Eds.), Landslide Science and Practice: Volume 6: Risk Assessment, Management and Mitigation. Springer Berlin Heidelberg, Berlin, Heidelberg, pp. 133–140. doi:10.1007/978-3-642-31319-6_19

Robertson, R.E.A., Latchman, J.L., Lynch, L., Dondin, F., Ash, C., Camejo, M., Christopher, T., Graham, O., Higgins, M., Jackson, V., Joseph, E., Juman, A., Juman, I., Nath, N., Ramsingh, C., Ramsingh, H., Ryan, G., Smith, P., Stewart, R., Stinton, A., 2015. Report on the 2015 unrest activity at Kick-'em-Jenny submarine volcano, Grenada.

Schmincke, H.-U., Shipboard, 1995. 2 . Background , Objectives , and Principal Results of Drilling the Clastic Apron of Gran Canaria (Vicap). Proc. Ocean Drill. Program, Initial Reports 157, 11–25.

Schmincke, H.-U., Sumita, M., 1998. Volcanic evolution of {G}ran {C}anaria reconstructed from apron sediments: synthesis of vicap project drilling. Proc. Ocean Drill. Program, Sci. Results 157, 443–469. doi:10.2973/odp.proc.sr.157.135.1998

Shepherd, J., 1988. Reporting in: Kick'em Jenny Volcano. Smithson. Inst. SEAN (Scientific Event Alert Network) Bull. 13, 9–10.

Shepherd, J.B., Robson, G.R., 1967. The source of the T phase recorded in the eastern Caribbean on October 24, 1965. Bull. Seismol. Soc. Am. 57, 227–234.

Siebert, L., Glicken, H., Ui, T., 1987. Volcanic hazards from Bezymianny- and Bandai-type eruptions. Bull. Volcanol. 49, 435–459. doi:10.1007/BF01046635

Sigurdsson, H., 1989. Submarine investigations in the crater of Kick'em Jenny volcano.

Bull. Sci. Event Alert Netw. 4, 45–49.

Sigurdsson, H., Carey, S., Wilson, D., 2006. Debris avalanche formation at Kick'em Jenny submarine volcano. World Scientific, Hackensack, NJ.

Sigurdsson, H., Shepherd, J.B., 1974. Amphibole-bearing basalts from the submarine volcano Kick'em-Jenny in the lesser antilles Island arc. Bull. Volcanol. 38, 1–20. doi:10.1007/BF02597097

Silver, E., Day, S., Ward, S., Hoffmann, G., Llanes, P., Driscoll, N., Appelgate, B., Saunders, S., 2009. Volcano collapse and tsunami generation in the Bismarck Volcanic Arc, Papua New Guinea. J. Volcanol. Geotherm. Res. 186, 210–222. doi:http://dx.doi.org/10.1016/j.jvolgeores.2009.06.013

Sinton, J.M., Detrick, R.S., 1992. Mid-ocean ridge magma chambers. J. Geophys. Res. Solid Earth 97, 197–216.

Skvortsov, A., Bornhold, B., 2007. Numerical simulation of the landslide-generated tsunami in Kitimat Arm, British Columbia, Canada, 27 April 1975. J. Geophys. Res. Earth Surf. 112, 1–12. doi:10.1029/2006JF000499

Smith, R.L., Bailey, R.A., 1968. Resurgent cauldrons. Geol. Soc. Am. Mem. 116, 613–662.

Smith, T.L., Batiza, R., 1989. New field and laboratory evidence for the origin of hyaloclastite flows on seamount summits. Bull. Volcanol. 51, 96–114. doi:10.1007/BF01081979

Smith, W.H., Sandwell, D., 1997. Global Sea Floor Topography from Satellite Altimetry and Ship Depth Soundings. Science (80-.). 277, 1956–1962.

doi:10.1126/science.277.5334.1956

Smolka, A., 2006. Natural disasters and the challenge of extreme events: risk management from an insurance perspective. Philos. Trans. R. Soc. A Math. Phys. Eng. Sci. 364, 2147–2165. doi:10.1098/rsta.2006.1818

Sparks, R.S.J., Barclay, J., Calder, E.S., Herd, R.A., Komorowski, J.-C., Luckett, R., Norton, G.E., Ritchie, L.J., Voight, B., Woods, A.W., 2002. Generation of a debris avalanche and violent pyroclastic density current on 26 December (Boxing Day) 1997 at Soufrière Hills Volcano, Montserrat. Geol. Soc. London, Mem. 21, 409–434. doi:10.1144/GSL.MEM.2002.021.01.18

Speight, M.R., Henderson, P.A., 2010. Marine ecology: concepts and applications. John Wiley & Sons.

Stothers, R.B., 1993. Flood basalts and extinction events. Geophys. Res. Lett. 20, 1399–1402.

Suleimani, E., Nicolsky, D.J., Haeussler, P.J., Hansen, R., 2011. Combined effects of tectonic and landslide-generated Tsunami Runup at Seward, Alaska during the Mw 9.2 1964 earthquake. Pure Appl. Geophys. 168, 1053–1074. doi:10.1007/s00024-010-0228-4

Szitkar, F., Dyment, J., Fouquet, Y., Choi, Y., Honsho, C., 2015a. Absolute magnetization of the seafloor at a basalt-hosted hydrothermal site: Insights from a deep-sea submersible survey. Geophys. Res. Lett. 42, 1046–1052.

Szitkar, F., Petersen, S., Caratori Tontini, F., Cocchi, L., 2015b. High-resolution magnetics reveal the deep structure of a volcanic-arc-related basalt-hosted

hydrothermal site (Palinuro, Tyrrhenian Sea). Geochemistry, Geophys. Geosystems 16, 1–12. doi:10.1002/2015GC005769

Talwani, M., Heirtzler, J.R., 1964. Computation of magnetic anomalies caused by two dimensional structures of arbitrary shape. Stanford University Publications of the Geological Sciences.

Tappin, D.R., Watts, P., Grilli, S.T., 2008. The Papua New Guinea tsuanmi of 17 July 1998: anatomy of a catastrophic event. Nat. Hazards Earth Syst Sci 8, 243–266.

Tatsumi, Y., 2005. The subduction factory: How it operates in the evolving Earth. GSA Today 15, 4–10. doi:10.1130/1052-5173(2005)015[4:TSFHIO]2.0.CO;2

Thébault, E., Finlay, C.C., Beggan, C.D., Alken, P., Aubert, J., Barrois, O., Bertrand, F., Bondar, T., Boness, A., Brocco, L., Canet, E., Chambodut, A., Chulliat, A., Coïsson, P., Civet, F., Du, A., Fournier, A., Fratter, I., Gillet, N., Hamilton, B., Hamoudi, M., Hulot, G., Jager, T., Korte, M., Kuang, W., Lalanne, X., Langlais, B., Léger, J.-M., Lesur, V., Lowes, F.J., Macmillan, S., Mandea, M., Manoj, C., Maus, S., Olsen, N., Petrov, V., Ridley, V., Rother, M., Sabaka, T.J., Saturnino, D., Schachtschneider, R., Sirol, O., Tangborn, A., Thomson, A., Tøffner-Clausen, L., Vigneron, P., Wardinski, I., Zvereva, T., 2015. International Geomagnetic Reference Field: the 12th generation. Earth, Planets Sp. 67, 1–19. doi:10.1186/s40623-015-0228-9

Tibaldi, A., Vezzoli, L., 1998. The space problem of caldera resurgence: an example from Ischia Island, Italy. Geol. Rundschau 87, 53–66.

Tivey, M.A., Johnson, H.P., 2002. Crustal magnetization reveals subsurface structure of

Juan de Fuca Ridge hydrothermal vent fields. Geology 30, 979–982.

Tivey, M.A., Johnson, H.P., 2001. High-resolution geophysical mapping of the hydrothermal vent systems at Endeavour Ridge, Juan de Fuca, in: AGU Fall Meeting Abstracts. p. 440.

Tivey, M.A., Johnson, H.P., 1989. High-Resolution Geophysical Studies of Oceanic Hydrothermal Systems. CRC Crit. Rev. Aquat. Sci.

Tivey, M.A., Johnson, H.P., Fleutelot, C., Hussenoeder, S., Lawrence, R., Waters, C., Wooding, B., 1998. Direct measurement of magnetic reversal polarity boundaries in a cross-section of oceanic crust. Geophys. Res. Lett. 25, 3631–3634. doi:10.1029/98GL02752

Tivey, M.A., Johnson, P.H., Salmi, M.S., Hutnak, M., 2014. High-Resolution Near-Bottom Vector Magnetic Anomalies Over Raven Hydrothermal Field, Endeavour Segment, Juan de Fuca Ridge. J. Geophys. Res. Solid Earth 19, 1–15. doi:10.1002/2014JB011223.Received

Tucker, M.E., 2009. Sedimentary petrology: an introduction to the origin of sedimentary rocks. John Wiley & Sons.

Twichell, D.C., Chaytor, J.D., ten Brink, U.S., Buczkowski, B., 2009. Morphology of late Quaternary submarine landslides along the U.S. Atlantic continental margin. Mar. Geol. 264, 4–15. doi:10.1016/j.margeo.2009.01.009

Vine, F.J., Matthews, D.H., 1963. Magnetic anomalies over oceanic ridges. Nature 4897, 947–949.

Voight, B., Komorowski, J.-C., Norton, G.E., Belousov, A.B., Belousova, M., Boudon,

G., Francis, P.W., Franz, W., Heinrich, P., Sparks, R.S.J., Young, S.R., 2002. The 26 December (Boxing Day) 1997 sector collapse and debris avalanche at Soufrière Hills Volcano, Montserrat. Geol. Soc. London, Mem. 21, 363–407. doi:10.1144/GSL.MEM.2002.021.01.17

Walter, T.R., Troll, V.R., 2000. Formation of caldera periphery faults : an experimental study. Bull. Volcanol. 63, 191–203. doi:10.1007/s004450100135

Watt, S.F.L., Jutzeler, M., Talling, P.J., Carey, S.N., Sparks, R.S.J., Tucker, M., Stinton, A.J., Fisher, J.K., Wall-Palmer, D., Hühnerbach, V., Moreton, S.G., 2015. New insights into landslide processes around volcanic islands from Remotely Operated Vehicle (ROV) observations offshore Montserrat. Geochemistry, Geophys. Geosystems 16, 2240–2261. doi:10.1002/2015GC005781

Watt, S.F.L., Talling, P.J., Vardy, M.E., Masson, D.G., Henstock, T.J., Hühnerbach, V., Minshull, T.A., Urlaub, M., Lebas, E., Friant, A. Le, Berndt, C., Crutchley, G.J., Karstens, J., 2012. Widespread and progressive seafloor-sediment failure following volcanic debris avalanche emplacement: Landslide dynamics and timing offshore Montserrat, Lesser Antilles. Mar. Geol. 323–325, 69–94. doi:http://dx.doi.org/10.1016/j.margeo.2012.08.002

Watts, A.B., Masson, D.G., 1995. A giant landslide on the north flank of Tenerife, Canary Islands. J. Geophys. Res. 100, 24487–24498. doi:10.1029/95JB02630

Watts, A.B., Peirce, C., Grevemeyer, I., Paulatto, M., Stratford, W., Bassett, D., Hunter, J.A., Kalnins, L.M., de Ronde, C.E.J., 2012. Rapid rates of growth and collapse of Monowai submarine volcano in the Kermadec Arc. Nat. Geosci 5, 510–515.

Watts, P., Grilli, S.T., Tappin, D.R., Fryer, G.J., 2005. Tsunami generation by submarine mass failure. II: Predictive equations and case studies. J. Waterw. Port Coast. Ocean Eng. 131, 298–310. doi:10.1061/(asce)0733-950x(2005)131:6(298)

Wessel, P., 2001. Global distribution of seamounts inferred from gridded Geosat/ERS-1 altimetry. J. Geophys. Res. Solid Earth 106, 19431–19441. doi:10.1029/2000JB000083

Wessel, P., 1997. Sizes and ages of seamounts using remote sensing: implications for intraplate volcanism. Science (80-.). 277, 802–805.

White, S.M., Crisp, J.A., Spera, F.J., 2006. Long-term volumetric eruption rates and magma budgets. Geochemistry, Geophys. Geosystems 7, 1–20. doi:10.1029/2005GC001002

Whitehouse, I.E., 1983. Distribution of large rock avalanche deposits in the central Southern Alps, New Zealand. New Zeal. J. Geol. Geophys. 26, 271–279. doi:10.1080/00288306.1983.10422240

Wiemer, G., 2014. On the role of volcanic material in submarine landslide initiation processes. Bremen, Universität Bremen, Diss., 2014.

Wilson, J.T., 1963. A possible origin of the Hawaiian Islands. Can. J. Phys. 41, 863–870.